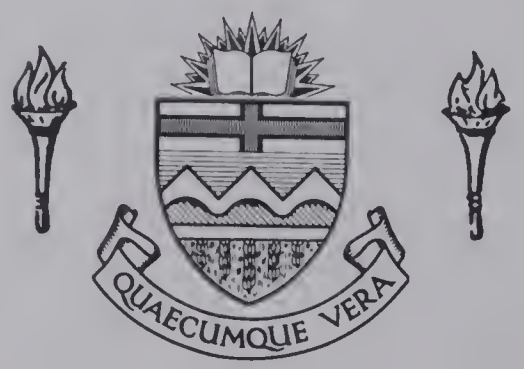

The University of Alberta
Printing Department
Edmonton, Alberta

THE UNIVERSITY OF ALBERTA

A MAGNETOTELLURIC STUDY OF RESISTIVITY ANISOTROPY

by

INDUPURU KOTA REDDY

A THESIS

SUBMITTED TO THE FACULTY OF GRADUATE STUDIES IN PARTIAL

FULFILLMENT OF THE REQUIREMENTS FOR THE DEGREE OF

MASTER OF SCIENCE

Department of Physics
Edmonton, Alberta

February, 1968.

UNIVERSITY OF ALBERTA

FACULTY OF GRADUATE STUDIES

The undersigned certify that they have read, and recommend to the Faculty of Graduate Studies for acceptance, a thesis entitled A MAGNETOTELLURIC STUDY OF RESISTIVITY ANISOTROPY, submitted by Indupuru Kota Reddy, in partial fulfillment of the requirements for the degree of Master of Science.

ABSTRACT

Magnetotelluric measurements in the frequency range 0.001 to 1 Hz were made at the University of Alberta Geophysical Observatory near Leduc, Alberta, as part of the crustal conductivity measurements in central and southern Alberta. The analog data obtained were converted into digital form and power spectral analyses using the Fast Fourier transform techniques were made on the digital data. The apparent resistivity curves obtained from the power spectral density estimates, and the polarization studies of horizontal electric and magnetic fields indicated the presence of strong resistivity anisotropy at the Observatory.

Apparent resistivity curves for several theoretical, anisotropic layered earth models were computed in order to match with the experimental curves. The results thus obtained indicated that the resistivity structure beneath the Observatory corresponds to a four layered anisotropic earth model, with the upper isotropic sedimentary section underlain by two anisotropic layers of the Precambrian basement. The total thickness of the anisotropic layers and the direction of the major axis of anisotropy were found to be 10 km and N 50° E respectively. A resistivity of 1000 ohm meters was obtained for the bottom layer.

ACKNOWLEDGEMENTS

I wish to express my sincere thanks to Professor D. Rankin, for suggesting the thesis topic and providing guidance and assistance throughout this investigation.

I am grateful to Mr. M.D. Burke for his assistance in operating the recording equipment and in digitizing the data, and to W.J. Peeples for his assistance in analysing the data. I am also thankful to G.S. Murthy for his help in preparing the manuscript of the thesis.

During the course of this research the author was supported by a Graduate Teaching Assistantship from the Department of Physics, University of Alberta, and by the National Research Council of Canada.

TABLE OF CONTENTS

LIST OF ILLUSTRATIONS

CHAPTER 1

INTRODUCTION

During the summer months of 1966 magnetotelluric measurements were carried out at several central and southern Alberta stations, in order to delineate the conductivity structure of the upper crust in these regions. During the same period continuous registration of magnetotelluric field variations had also been made at the University of Alberta Geophysical Observatory (53^{o} 13' N; 113^{o} 21' W), so as to facilitate the studies on magnetotelluric source fields. The latter measurements were also intended to determine the conductivity structure at the Observatory, which is to be the reference station for future magnetotelluric studies at the University of Alberta. The subject matter of this thesis is mainly the determination and interpretation of the conductivity structure at the Observatory, from the magnetotelluric data.

1.1. Geology at the Measuring Site

The Geophysical Observatory of the University of Alberta, where the present magnetotelluric measurements were made, is situated in the central plains of Alberta. The Precambrian shield in the central plains is overlain by about 2.5 km of flat-lying sediments. The sedimentary section in this region has been fairly well studied by geophysical and geological

methods in the course of exploration for oil. A typical cross-section of the sediments, with well log resistivities is illustrated in Figure 1.

Garland and Burwash (1959) have studied the petrology of the Precambrian shield using well log samples and gravity anomalies. Their lithological map of the Precambrian basement is depicted in Figure 2 on which is superimposed the location of the Observatory. Vozoff et al (1963) have carried out magnetotelluric measurements in this area and found that no significant resistivity anisotropy exists in the sedimentary section. No crustal seismic data are available for this location but the seismic crustal studies by Richards and Walker (1959), about 200 miles farther south, gave depths of 29 km and 43 km to the Conrad and Mohorovicic discontinuities. They also predicted heterogeneity in the upper or "granitic" layer.

1.2. Historical Review of the Magnetotelluric Method

Almost simultaneously Tikhonov (1950), Kato and Kikuchi (1950) and Rikitake (1950, 1951) observed the existence of a correlation between the geomagnetic and telluric field variations at the surface of the earth, and investigated methods for exploring to great depths. However, it was not until Cagniard's (1953) classic paper that the method attracted serious attention. Cagniard presented a method of interpreting the results of magnetotelluric measurements as

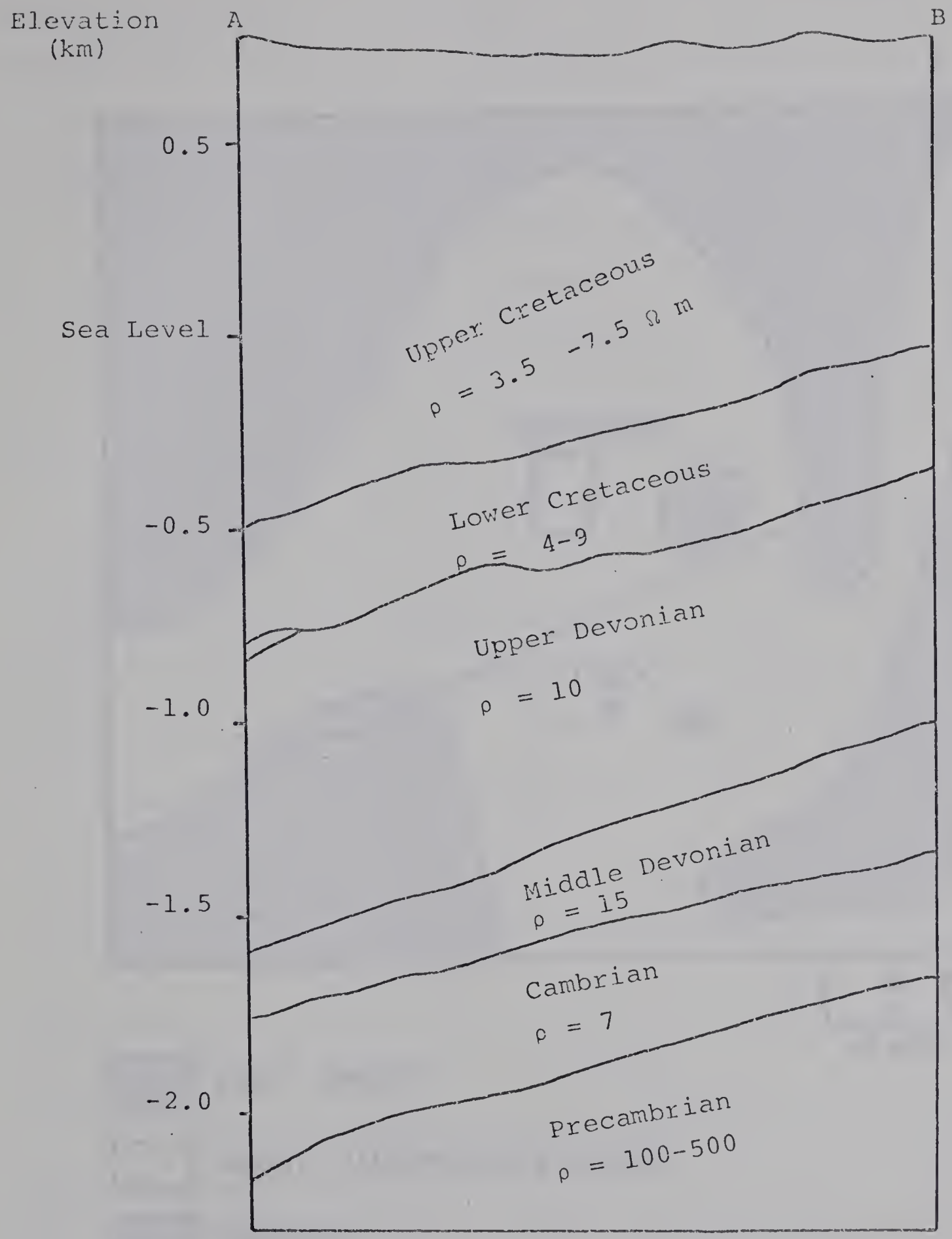

Figure 1: Geological cross-section AB (Figure 2) of Edmonton area, with typical well-log resistivities (after Ellis, 1964)

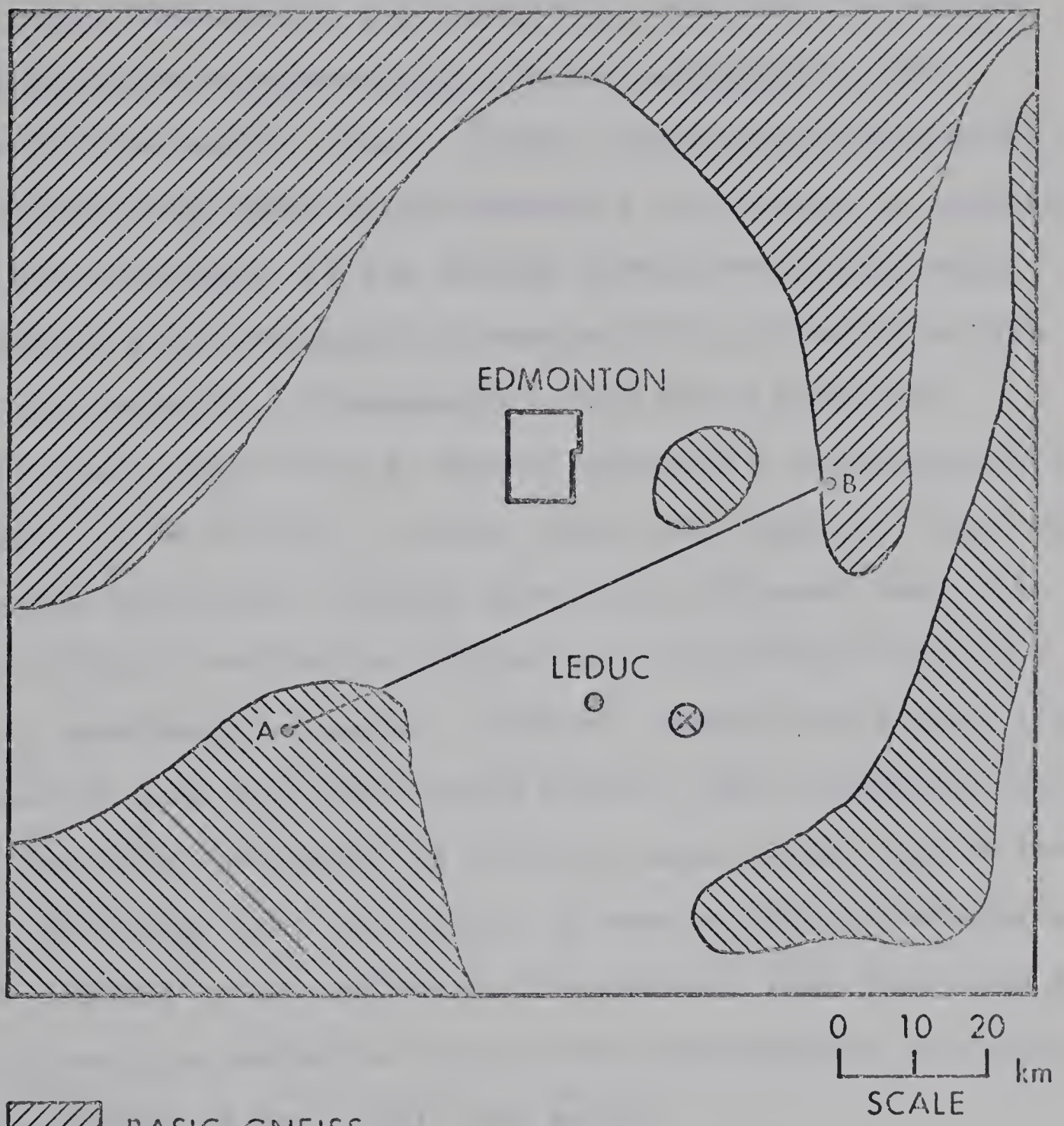

Figure 2: Lithology of the Precambrian basement as inferred from well samples and gravity anomalies (after Garland and Burwash, 1959)

applied to geophysical exploration. Cagniard's method assumes that the earth is horizontally stratified with each layer being homogeneous and isotropic, and that the source fields are plane electromagnetic waves impinging on the surface of the earth. Wait (1954), questioning Cagniard's assumptions, has shown that Cagniard's results for a layered earth are valid only if the fields themselves do not vary appreciably in a horizontal distance of the order of a skin depth in the earth. Consequently, the field should be uniform over a wide area to permit Cagniard's interpretative procedure to be applied. Price (1962) has indicated that the limitation mentioned, becomes much more stringent when the magnetotelluric method is applied to a stratified earth in certain important instances. However, Madden and Nelson (1964), considering some realistic earth models, have concluded that the plane-wave assumption is valid in most cases. Srivastava (1965) has shown that the effect of wavelength of the source can be assumed to be negligible for periods less than 1000 sec, when determining moderate resistivity distribution in shallow regions (10 to 20 km) within the earth.

Following Cagniard's methods, magnetotelluric measurements have been carried out successfully by several investigators (Cantwell, 1960; Wiese, 1962; Srivastava et al., 1963; Vozoff et al., 1963; Tikhonov and Berdichevskii, 1966; Hopkins and Smith, 1966; and others). But problems have arisen in interpreting the magnetotelluric data in areas of

lateral conductivity variations. Chetaev (1960), Kovtun (1961), Rokityanski (1961), Cantwell (1960), Bostick and Smith (1962), and others have suggested methods to interpret magnetotelluric data over anisotropic or inhomogeneous earth. Theoretical studies for two dimensional inhomogeneities have been made by Neves (1957), d'Erceville and Kunetz (1962), Rankin (1962), Weaver (1963) and Mann (1964). Analog model studies over two and three dimensional bodies have been made by Rankin et al. (1965), Dosso (1966) and others.

1.3. Outline of Thesis

In Chapter 2 electromagnetic theory applied to a layered half-space and Cagniard's magnetotelluric effect are studied. The magnetotelluric theory over n-layer anisotropic earth models, and a method of obtaining apparent resistivity curves for such models are presented.

A brief description of the magnetotelluric measuring equipment and the techniques of handling the magnetotelluric data are given in Chapter 3.

In Chapter 4 polarization diagrams and apparent resistivity curves are presented. These apparent resistivity curves are interpreted in terms of a four-layered anisotropic earth. An interpretation of the resistivity structure in terms of local geologic structures is attempted. Chapter 4 is followed by conclusions and suggestions for further work, references and three Appendices.

CHAPTER 2

MAGNETOTELLURIC THEORY

2.1. Intrinsic Impedance of a Semi-infinite Isotropic Half-Space

For the case of plane electromagnetic waves impinging on a homogeneous isotropic earth, the geometry of the ionospheric layers and the frequencies of interest (viz. 0.001 Hz to 1 Hz) allow the effect of the earth's curvature to be neglected. Because of the enormous contrast between the velocity of propagation of electromagnetic waves in the air and in the earth, the refracted wave will propagate vertically downward regardless of the angle of incidence. Furthermore the component of current across the surface can be neglected. In general the displacement current is negligible compared to the conduction current in earth materials, in the frequency range of interest. The magnetic permeability in most cases of interest can be taken to be that of free space ($\mu = 1$). If in addition, one considers a single Fourier component of general electromagnetic disturbance, the time dependence can be written as $e^{i\omega t}$ and Maxwell's equations in em system of units can be written as

$$\text{curl } \vec{H} = 4\pi \vec{J} = 4\pi\rho \vec{E} \qquad (2.1)$$

$$\text{curl}\ \vec{E} = -\ i\ \omega\ \vec{H} \tag{2.2}$$

$$\text{div}\ \vec{H} = 0 \tag{2.3}$$

and the Helmholtz (or diffusion) equation for the electric field $\vec{E}$ in the medium becomes

$$\nabla^2\ \vec{E} - k^2\ \vec{E} = 0 \tag{2.4}$$

where $$k^2 = 4\ \pi\ i\ \omega\ \sigma\ . \tag{2.5}$$

Considering a cartesian coordinate system with the x-y plane on the earth's surface and z vertically downwards, and assuming that the electric vector $\vec{E}$ in the plane wave is polarized in the x direction and the magnetic vector $\vec{H}$ in the y direction, the diffusion equation (2.4) can be written as

$$\frac{d^2E_x}{dz^2} = k^2\ E_x. \tag{2.6}$$

The solution of Equation (2.6) in the case of a semi-infinite medium ($z \to \infty$), has the form

$$E_x = A\ e^{-kz}\ . \tag{2.7}$$

From Equation (2.2)

$$H_y = -\ \frac{1}{i\omega}\ \frac{dE_x}{dz} \tag{2.8}$$

Substituting E_x value from Equation (2.7) in Equation (2.8), we have

$$H_y = \frac{k}{i\omega} A e^{-kz} . \qquad (2.9)$$

Then the intrinsic impedance of the medium, for the plane wave, as defined by Schelkunoff (1943), is

$$Z = \left.\frac{E_x}{H_y}\right|_{z = 0} = (2\sigma T)^{-\frac{1}{2}} e^{-i\pi/4} \qquad (2.10)$$

From the above relation one can see that the intrinsic impedance is a function of the conductivity of the medium σ, and the period of the wave T, and for a plane wave impinging on a homogeneous, isotropic semi-infinite medium, the phase of H_y is retarded by $\pi/4$ radians with respect to that of E_x.

The resistivity of the medium ρ can be expressed in terms of the intrinsic impedance as

$$\rho = 2T \left|\frac{E_x}{H_y}\right|^2 \qquad (2.11)$$

which is the basic equation developed by Cagniard (1953) for the magnetotelluric method of exploration. In practical em system of units Equation (2.11) is written as

$$\rho = 0.2 \; T \left|\frac{E_x}{H_y}\right|^2 \qquad (2.12)$$

where

ρ = resistivity in ohm-meters

T = period of magnetotelluric disturbance in seconds

E_x = disturbance in the electric field in mv/km

H_y = disturbance in the magnetic field in gammas

The depth of penetration (or skin depth) is defined as the depth p in kilometers, where the amplitude is reduced to fraction 1/e of what it is on the surface and is given by

$$p = \frac{1}{2\pi} \sqrt{10\rho T} \qquad (2.13)$$

2.2. Intrinsic Impedance of an n-layer Homogeneous Isotropic Half-space

Cagniard (1953) obtained formulae for the intrinsic impedance of two and three layered models and provided methods to interpret experimentally observed curves in terms of a two layer earth model, by curve matching techniques. Yungul (1961) presented magnetotelluric sounding curves over three layer earth models and gave interpretation procedures. Srivastava (1967) published a catalog of apparent resistivity and phase curves over two and three layered earth models.

Berdichevskii (1960) extended Cagniard's theory, for two and three layered earth models, to an n-layered isotropic half-space and obtained the following relation for the

intrinsic impedance

$$Z = \left.\frac{E_x}{H_y}\right|_{z=0} = -\frac{i\omega}{k_1} \coth\left\{k_1 h_1 + \operatorname{arcth}\left[\frac{k_1}{k_2} \coth\left(k_2 h_2 + \ldots + \operatorname{arcth}\left[\frac{k_{n-2}}{k_{n-1}} \coth\left(k_{n-1} h_{n-1} + \operatorname{arcth}\frac{k_{n-1}}{k_n}\right)\right] \ldots\right)\right]\right\} \qquad (2.14)$$

where

k_m = wave number in the m^{th} layer, given by $(-4\pi i \omega / \rho_m)^{\frac{1}{2}}$

h_m = thickness of the m^{th} layer

ρ_m = resistivity of the m^{th} layer.

It becomes somewhat difficult to compute intrinsic impedance using Equation (2.14), particularly when the source dimensions are introduced and the number of layers in the model is greater than three.

In order to compute the intrinsic impedance and corresponding apparent resistivity for an n-layered isotropic half-space, avoiding the rather laborious methods of the previously mentioned authors, a straightforward iterative method which produces the apparent resistivity curves for complex models with relative ease is presented here.

Again, considering the rectangular coordinate system with the surface of the earth at z = 0 in the x-y plane, and

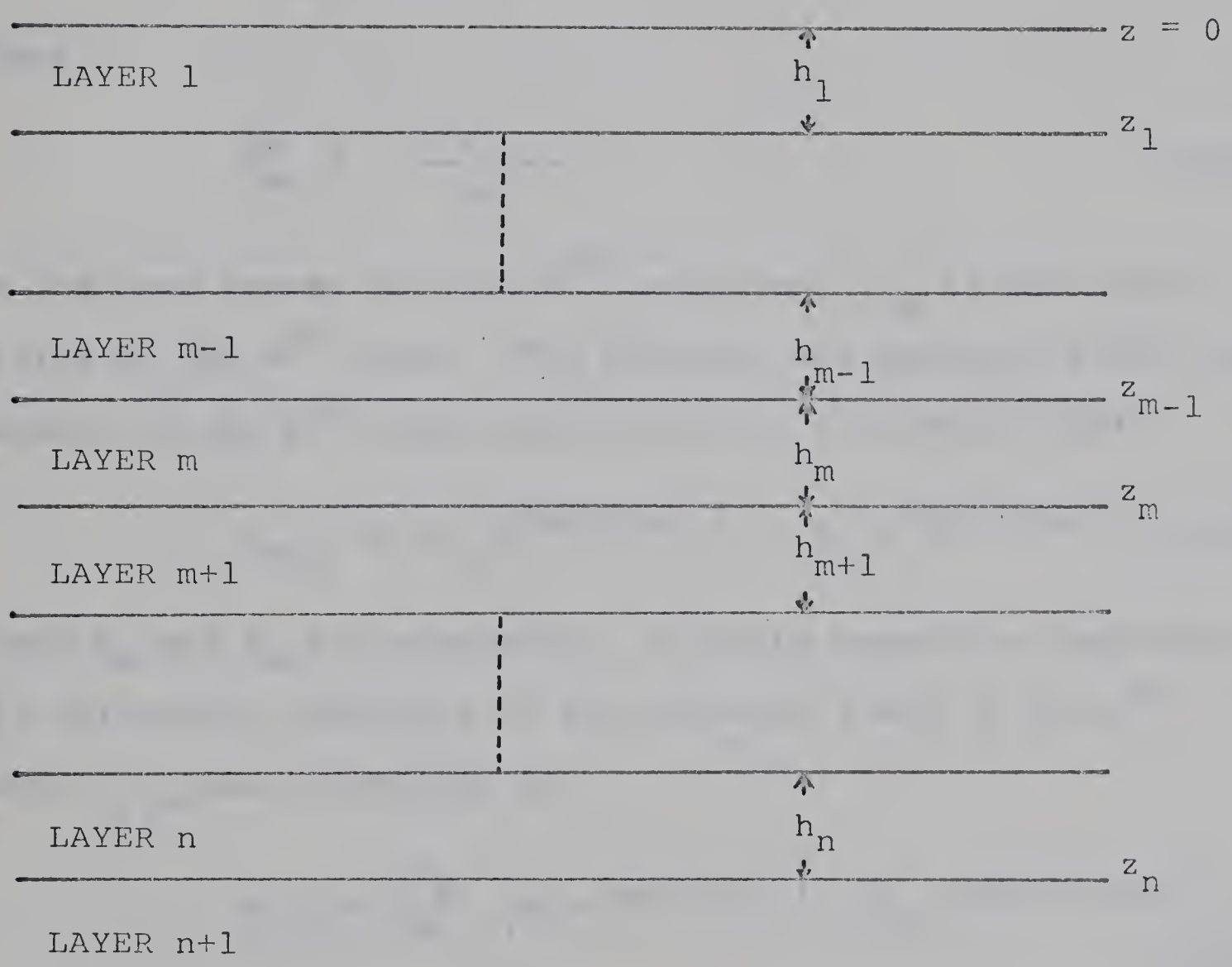

Figure 3: n + 1 layer model

assuming that the model consists of n homogeneous isotropic plane parallel layers underlain by a homogeneous isotropic half-space (Fig. 3), the diffusion Equation (2.6), in each layer is written as

$$\frac{d^2 E_{x,m}}{dz^2} = k_m^2 \, E_{x,m} \tag{2.15}$$

where

$$k_m^2 = \frac{4 \pi i \omega}{\rho_m} \tag{2.16}$$

is the wave number for the m^{th} layer, and ρ_m is the resistivity of the m^{th} layer. The electric and magnetic field components in the m^{th} layer can be written as (Jones, 1964)

$$E_{x,m} = A_m \, e^{k_m (z - z_{m-1})} + B_m \, e^{-k_m (z - z_{m-1})} \tag{2.17}$$

where A_m and B_m are constants. By using Maxwell's equations, the horizontal component of the magnetic field in the m^{th} layer $H_{y,m}$ can be written as

$$H_{y,m} = \frac{-k_m}{i\omega} \left| A_m \, e^{k_m (z - z_{m-1})} - B_m \, e^{-k_m (z - z_{m-1})} \right| . \tag{2.18}$$

Applying the boundary condition, viz., the tangential components of electric and magnetic field vectors are continuous at the boundary $z = z_m$, one gets from Equations (2.17) and

(2.18)

$$A_m \, e^{k_m h_m} + B_m \, e^{-k_m h_m}$$

$$= A_{m+1} \, e^{k_{m+1} h_m} + B_{m+1} \, e^{-k_{m+1} h_m} \qquad (2.19)$$

$$A_m \, e^{k_m h_m} - B_m \, e^{-k_m h_m}$$

$$= \frac{k_{m+1}}{k_m} \left| A_{m+1} \, e^{k_{m+1} h_m} - B_{m+1} \, e^{-k_{m+1} h_m} \right| . \qquad (2.20)$$

Adding Equation (2.19) to Equation (2.20), one gets

$$A_m = \frac{k_m + k_{m+1}}{2 k_m} A_{m+1} \, e^{(k_{m+1} - k_m) h_m} + \frac{k_m - k_{m+1}}{2 k_m} B_{m+1} \, e^{-(k_{m+1} + k_m) h_m} \qquad (2.21)$$

and subtracting Equation (20) from Equation (19)

$$B_m = \frac{k_m - k_{m+1}}{2 k_m} A_{m+1} \, e^{(k_{m+1} + k_m) h_m}$$

$$+ \frac{k_m + k_{m+1}}{2} B_{m+1} \, e^{-(k_{m+1} - k_m) h_m} \qquad (2.22)$$

If the lower boundary of the $(n+1)^{th}$ layer extends to infinity ($h_{n+1} \to \infty$), one can start in the nether world with

$$A_{n+1} = 0, \quad B_{n+1} = 1, \qquad (2.23)$$

and we have very simple expressions for A_n and B_n, viz.

$$A_n = \frac{k_n - k_{n+1}}{2 k_n} e^{-(k_{n+1} + k_n)h_n} \tag{2.24}$$

$$B_n = \frac{k_n + k_{n+1}}{2 k_n} e^{-(k_{n+1} - k_n)h_n} \tag{2.25}$$

In the first layer

$$A_1 = \frac{k_2 + k_1}{2 k_1} A_2 e^{(k_2-k_1)h_1} + \frac{k_1 - k_2}{2 k_1} B_2 e^{-(k_2+k_1)h_1} \tag{2.26}$$

$$B_1 = \frac{k_1 - k_2}{2 k_1} A_2 e^{(k_2+k_1)h_1} + \frac{k_2 + k_1}{2 k_1} B_2 e^{-(k_2-k_1)h_1} \tag{2.27}$$

At the surface (z = 0)

$$E_x = A_1 + B_1 \tag{2.28}$$

$$H_y = \frac{-k_1}{i\omega} \left| A_1 - B_1 \right| . \tag{2.29}$$

The intrinsic impedance for an n-layered homogeneous isotropic half-space is then given by

$$Z = \left. \frac{E_x}{H_y} \right|_{z = 0} = - \frac{i\omega}{k_1} \frac{A_1 + B_1}{A_1 - B_1} \tag{2.30}$$

and the apparent resistivity in practical electromagnetic units is

$$\rho^a = 0.2 \; T \left| \frac{E_x}{H_y} \right|^2 \qquad (2.31)$$

Thus starting from Equation (2.23) one obtains Equations (2.26) and (2.27) by utilizing Equations (2.21) and (2.22).

Wait (1954) investigating the effect of non-plane wave sources on magnetotelluric theory, has shown that for magnetotelluric oscillations of frequency 0.1 Hz on a homogeneous earth of conductivity $\sigma = 10^{-3}$ mho/m, the spatial variations of E_x and H_y within a region of radius approximately 35 km must be small, otherwise corrections for second and higher order spatial derivatives of the source fields must be applied to Cagniard's plane wave theory for magnetotelluric fields. He has also pointed out that if the micro-pulsation sources were in a lower ionosphere at an altitude of 100 km, corrections would be important for frequencies less than 0.1 Hz.

Price (1962) has investigated the effect of the source dimensions on the intrinsic impedance E_x/H_y. For a homogeneous earth of conductivity σ, he found that

$$\frac{E_x}{H_y} = \frac{i\omega}{\theta} \qquad (2.32)$$

where

$$\theta^2 = \nu^2 + 4 \pi i \sigma \omega \qquad (2.33)$$

and ν is a separation constant which has a dimension L^{-1}.

According to Price $2\pi/\nu$ represents the linear dimension of the source field. He has also estimated the values of ν, and found that they range from 1.6×10^{-7} cm^{-1} for global fields to 1.6×10^{-5} cm^{-1} for local fields.

Taking into account the dimensions of the source field, the intrinsic impedance of n-layer, homogeneous, isotropic half-space can be written from equations (2.30), (2.32) and (2.33), as

$$Z_s = \left.\frac{E_x}{H_y}\right|_{z=0} = -\frac{i\omega}{\theta}\,\frac{A_1 + B_1}{A_1 - B_1} \qquad (2.34)$$

where $$\theta = \left[\left\{(\alpha^4 + \nu^4)^{\frac{1}{2}} + \nu^2\right\}^{\frac{1}{2}} + i\left\{(\alpha^4 + \nu^4)^{\frac{1}{2}} - \nu^2\right\}^{\frac{1}{2}}\right] / \sqrt{2} \qquad (2.35)$$

and $\alpha^2 = 4\,\pi\,\sigma\,\omega$.

Subscript s in Equation (2.34) indicates that the effect of source field is included. The apparent resistivity ρ_s^a, from Equation (2.31) and (2.34) is written as

$$\rho_s^a = 0.2\,T\,|Z_s|^2 \qquad (2.36)$$

A program has been written for the IBM 360/67 digital computer to compute apparent resistivity curves for n-layered earth models. One such model together with apparent

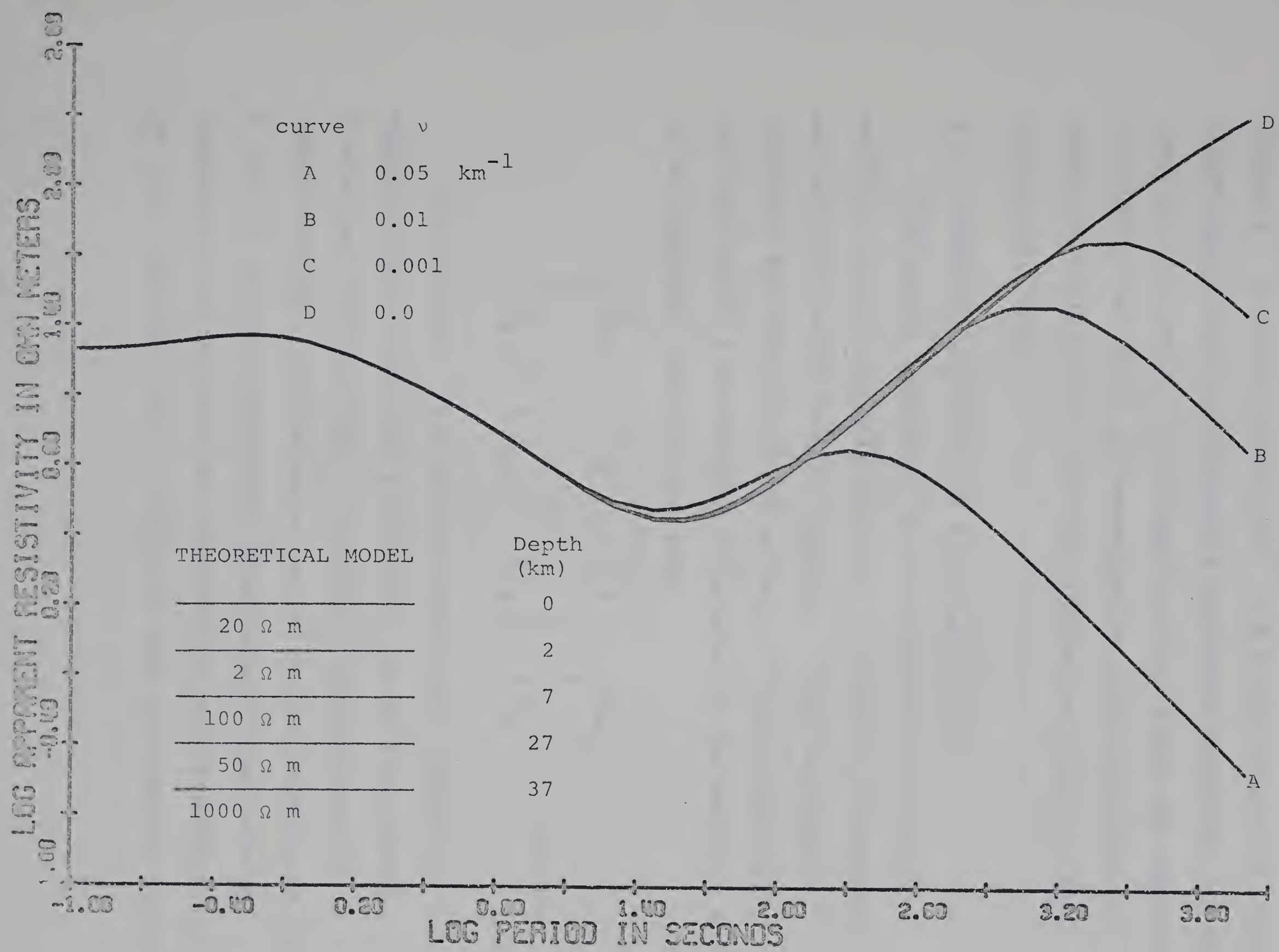

Figure 4: Computed apparent resistivity curves for a five layered earth model for various values of source dimension ν

resistivity curves for various values of ν is depicted in Figure 4. It may be noted that $\nu = 0$ (the source is infinitely large) corresponds to Cagniard's plane wave solution. In the rest of this thesis, ν is taken as zero, since the frequencies of interest and depth of investigation allow the effect of source dimension to be neglected (Madden and Nelson, 1964; Srivastava, 1965).

2.3. Intrinsic Impedance of Anisotropic Media

The scalar impedance, as developed in the previous section, allow interpretations only in terms of homogeneous and isotropic earth models. Cantwell (1960) developed a procedure for determining the effects of anisotropy and/or two dimensional inhomogeneous structures in the earth in terms of an impedance tensor of the form

$$\begin{vmatrix} E_x \\ E_y \end{vmatrix} = \begin{vmatrix} Z_{11} & Z_{12} \\ Z_{21} & Z_{22} \end{vmatrix} \begin{vmatrix} H_x \\ H_y \end{vmatrix} \qquad (3.27)$$

The electric field in one direction may depend on magnetic field variations parallel to, as well as perpendicular to, its direction. A method of calculating the tensor elements involves computing the Fourier components of $\vec{E}$ and $\vec{H}$ for two independent observations, then solving Equation (2.37) for both the observations simultaneously for the four elements. Swift (1967) has made an extensive study

on the characteristics of theoretical and measured impedance tensors.

Bostick and Smith (1962) have used the admittance tensor, defined by $\vec{H}_i = Y_{ij} \vec{E}_j$, rather than the impedance tensor and found that a rotation of the measuring axis to minimize the main diagonal terms in the impedance tensor yields a reasonably consistent estimate of the direction and magnitude of a major inhomogeneity in the apparent resistivity profile.

Mann (1965) has analyzed the problem of plane wave incidence on an anisotropic earth, and pointed out there exist two skin depths (Appendix 1) corresponding to two principal directions of anisotropy, and the impedance functions obtained at the surface are highly dependent on polarization as well as on anisotropy.

O'Brien and Morrison (1967) have studied the behaviour of electromagnetic fields in an n-layered anisotropic half-space, and have obtained the following equations for the total components of electric and magnetic fields in the m^{th} layer, where the axes of anisotropy lie in the x-y plane. The geometry is shown in Figure 5.

$$H_x^m = \frac{k_1^m}{\omega} P_m \tan \theta_m + \frac{k_2^m}{\omega} Q_m$$

$$H_y^m = \frac{k_1^m}{\omega} P_m - \frac{k_2^m}{\omega} Q_m \tan \theta_m$$

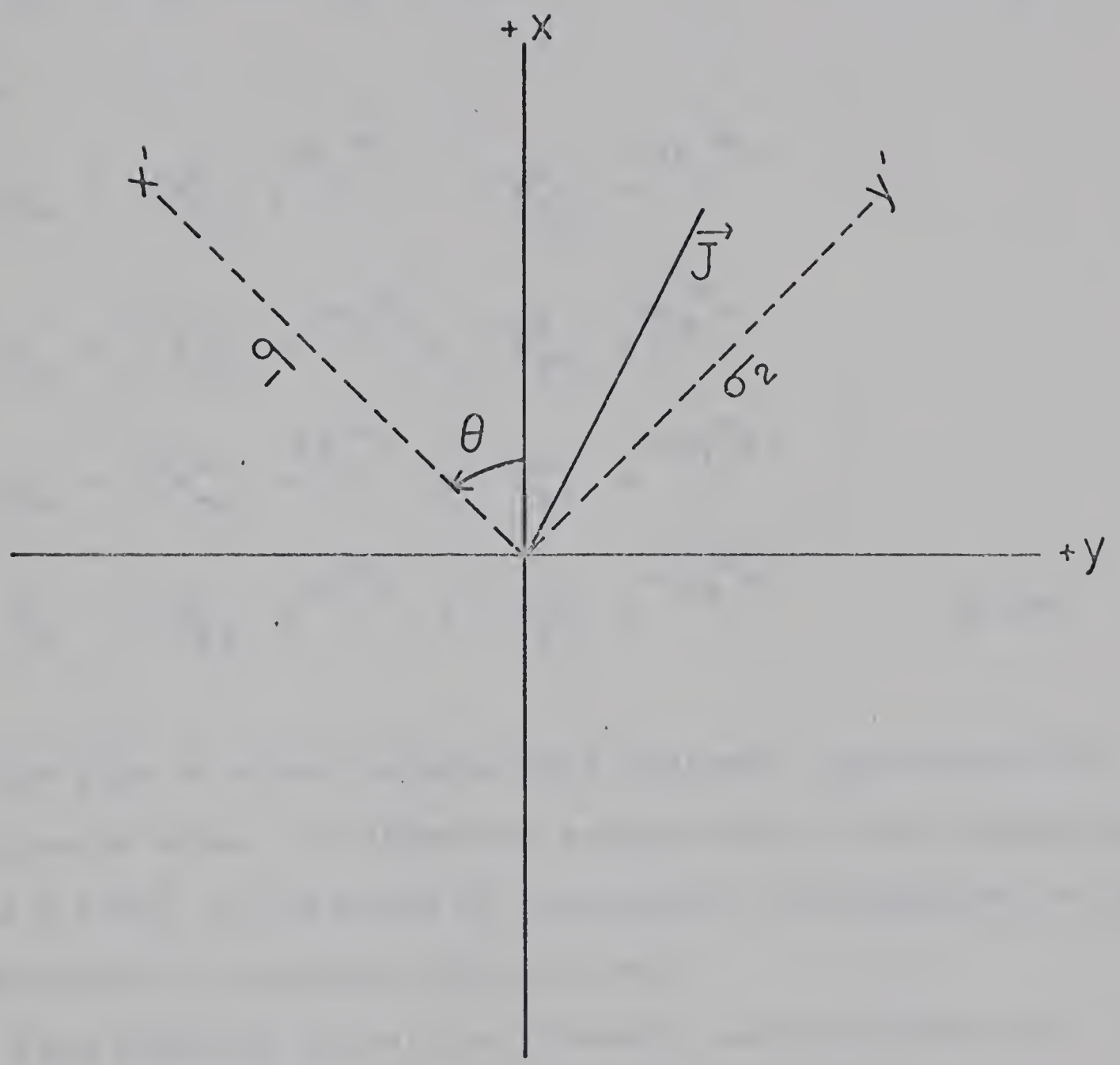

Figure 5: Relationship of conductivity anisotropy to coordinate axes

$$E_x^m = R_m + \tan \theta_m \, S_m$$

$$E_y^m = R_m \tan \theta_m + S_m \qquad (2.38)$$

where

$$P_m = {}^{+}E_{x1}^m \, e^{ik_1{}^m z} - {}^{-}E_{x_1}^m \, e^{-ik_1{}^m z}$$

$$Q_m = {}^{-}E_{y2}^m \, e^{-ik_2{}^m z} - {}^{+}E_{y2}^m \, e^{ik_2{}^m z}$$

$$R_m = {}^{+}E_{x1}^m \, e^{ik_1{}^m z} + {}^{-}E_{x1}^m \, e^{-ik_1{}^m z}$$

$$S_m = {}^{+}E_{y2}^m \, e^{ik_2{}^m z} + {}^{-}E_{y2}^m \, e^{-ik_2{}^m z} \qquad (2.39)$$

and the plus or minus superscripts indicate propagation in the plus or minus z direction respectively, where subscripts 1 and 2 refer to the modes of propagation corresponding to the two principal directions of anisotropy.

From Equation (2.38) the boundary conditions may be expressed in matrix form, as

$$\left|T^{m-1}\right| \begin{vmatrix} {}^{+}E_{x1}^{m-1} \\ {}^{-}E_{x1}^{m-1} \\ {}^{+}E_{y2}^{m-1} \\ {}^{-}E_{y2}^{m-1} \end{vmatrix} = \left|T^m\right| \begin{vmatrix} {}^{+}E_{x1}^m \\ {}^{-}E_{x1}^m \\ {}^{+}E_{y2}^m \\ {}^{-}E_{y2}^m \end{vmatrix} \qquad (2.40)$$

where

$$T^m = \begin{vmatrix} k_1^m \tan\theta_m e^{ik_1^m z_m} & k_1^m \tan\theta_m e^{-ik_1^m z_m} & -k_2 e^{ik_2^m z_m} & k_2^m e^{-ik_2^m z_m} \\ k_1^m e^{ik_1^m z_m} & -k_1^m e^{-ik_1^m z_m} & k_2^m \tan\theta_m e^{ik_2^m z_m} & -k_2^m \tan\theta_m e^{-ik_2^m z_m} \\ e^{ik_1^m z_m} & e^{ik_1^m z_m} & \tan\theta_m e^{ik_2^m z_m} & \tan\theta_m e^{-ik_2^m z_m} \\ -\tan\theta_m e^{ik_1^m z_m} & -\tan\theta e^{-ik_1^m z_m} & e^{ik_2^m z_m} & e^{-ik_2^m z_m} \end{vmatrix} \quad (2.41)$$

and T^{m-1} is identical except that all superscripts are changed to m-1 and the subscripts on θ only are changed to m-1.

The electric field components in the $m-1^{th}$ layer may be determined from Equation (2.41), and they may be written in matrix form, as

$$\left|E^{m-1}\right| = \left|A^{m}_{j,1}\right| \left|E^{m}\right| \qquad (2.42)$$

where

$$A^{m}_{j,1} = \left|T^{m-1}\right|^{-1} \left|T^{m}\right| \qquad (2.43)$$

For the (n+1) layer model of Figure 3, the surface (z = 0) electric fields are given in terms of the $\left|E^{m+1}\right|$, propagated into the half-space, by

$$\left|E^{1}\right| = \left|A^{1}_{j,1}\right| \left|E^{n+1}\right| \qquad (2.44)$$

where

$$\left|A^{1}_{j,1}\right| = \left|A^{2}_{j,1}\right| \left|A^{3}_{j,1}\right| \ldots \left|A^{m}_{j,1}\right| \ldots \left|A^{n+1}_{j,1}\right| \qquad (2.45)$$

and $|A_{j,1}|$ is defined in Equation (2.43).

The surface magnetic fields can be computed from the surface electric fields by Equations (2.38). Then the impedances and hence the apparent resistivities in the x and y directions can be calculated using Equations (2.10) and (2.12) respectively.

Due to the computational difficulties involved in a general solution, O'Brien and Morrison (1967) considered only

the case where θ is a constant, independent of depth.

Since the two modes of propagation for a single layer anisotropy are independent in the directions of principal axes, it is valid to treat a single layer anisotropy or a multilayered anisotropy for which the principal directions are the same, in a straight forward manner with computational ease, to obtain the impedances, and hence the apparent resistivities at the surface.

Considering a model consisting of an isotropic upper layer, two intermediate anisotropic layers and isotropic bottom layer extending to infinity (Figure 6) and representing the resistivities along the principal axes 1 and 2 in each layer by ρ_1 and ρ_2, the electric and magnetic field components E_1 and E_2, H_1 and H_2 can be obtained by using the formulae (2.28) and (2.29). The apparent resistivities ρ^a_{12} and ρ^a_{21} in the two principal directions, are then given by Equation (2.31). The apparent resistivities ρ^a_{xy} and ρ^a_{yx} along any measuring axes x and y may then be obtained by the relation (2.31)

$$\rho^a_{xy} = 0.2\ T\left|\frac{E_x}{H_y}\right|^2, \quad \rho^a_{yx} = 0.2\ T\left|\frac{E_y}{H_x}\right|^2 \qquad (2.46)$$

where

$$\begin{vmatrix} E_x \\ E_y \end{vmatrix} = |A| \begin{vmatrix} E_1 \\ E_2 \end{vmatrix}, \quad \begin{vmatrix} H_x \\ H_y \end{vmatrix} = |B| \begin{vmatrix} H_1 \\ H_2 \end{vmatrix}, \qquad (2.47)$$

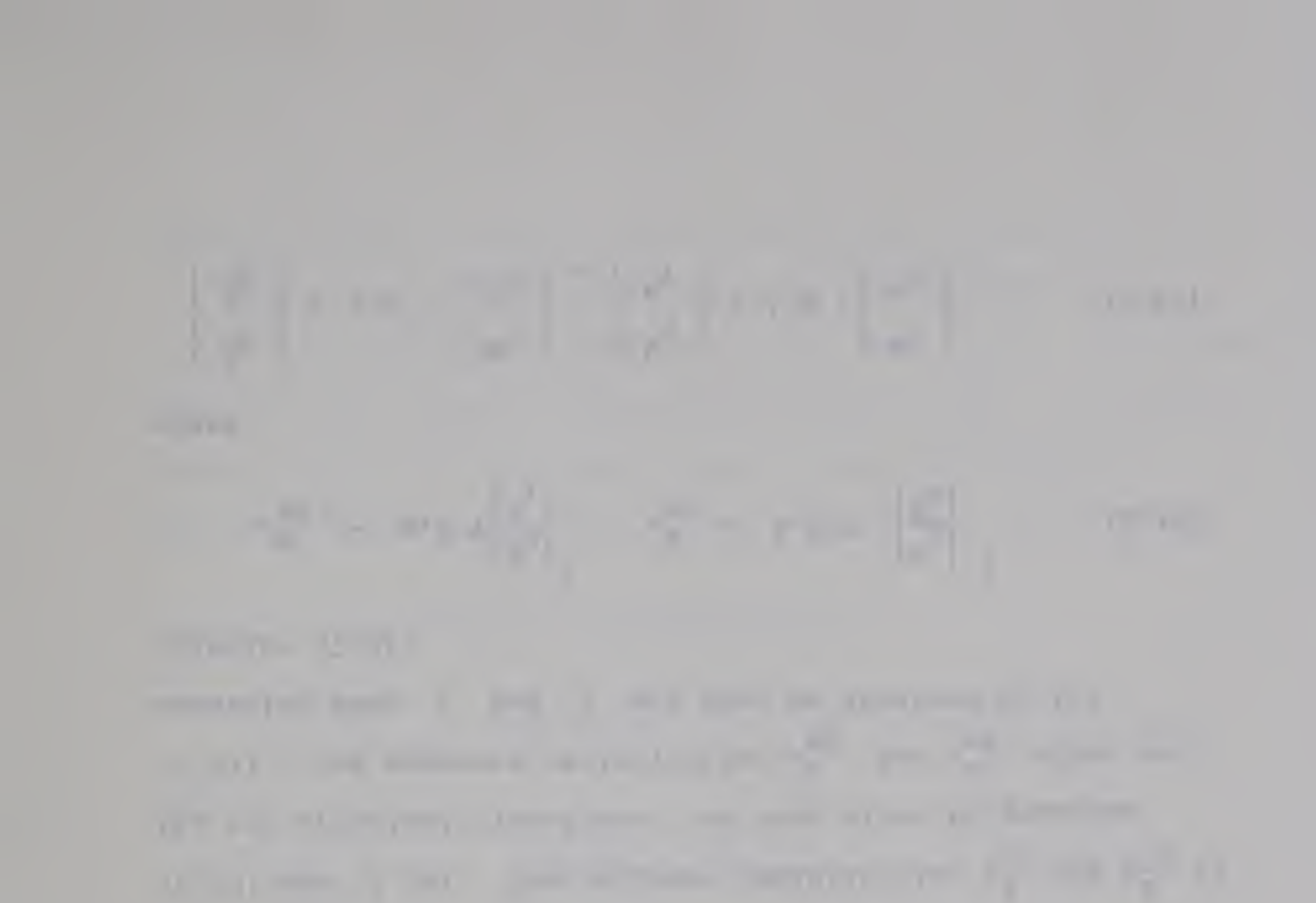

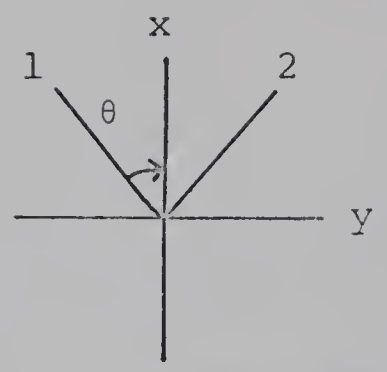

	Depth (km)
$\rho_1 = \rho_2 = 8\ \Omega$ m	2.5
$\rho_1 = 400\ \Omega$ m, $\rho_2 = 200\ \Omega$ m	4.5
$\rho_1 = 60\ \Omega$ m $\quad \rho_2 = 10\ \Omega$ m	12.5
$\rho_1 = \rho_2 = 1000\ \Omega$ m	

Figure 6: Four layered anisotropic earth model

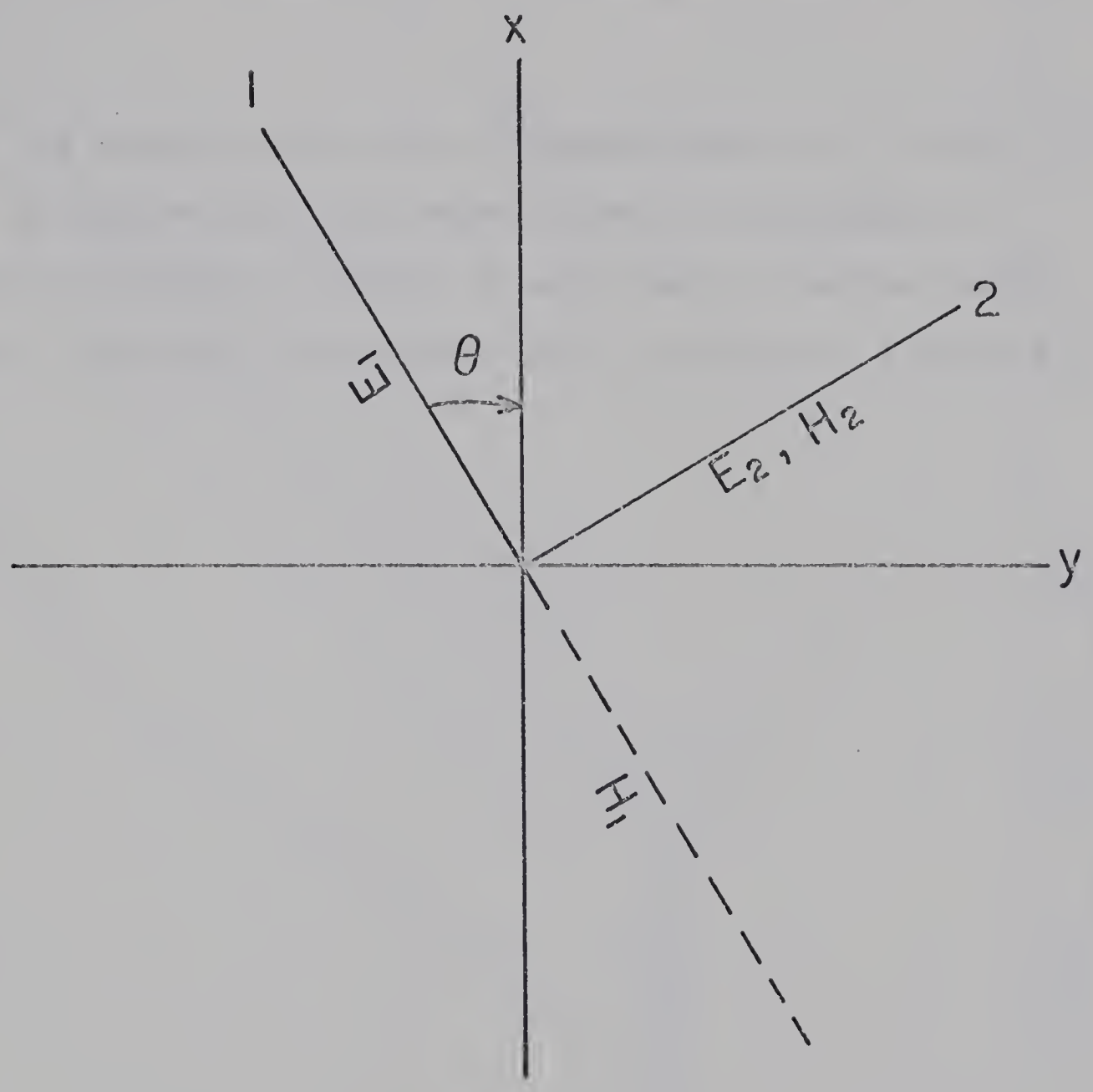

Figure 7: Relationship of electric and magnetic field components at the surface of anisotropic earth (1 and 2 are the principal directions of anisotropy)

$$|A| = \begin{vmatrix} \cos\theta & -\sin\theta \\ \sin\theta & \cos\theta \end{vmatrix}, \quad |B| = \begin{vmatrix} \cos\theta & \sin\theta \\ -\sin\theta & \cos\theta \end{vmatrix} \qquad (2.48)$$

and θ is the angle to the axis of measurement x in the clockwise direction from the major axis of anisotropy 1. The geometry is shown in Figure 7 and a set of master curves obtained for the model considered here is given in Figure 8.

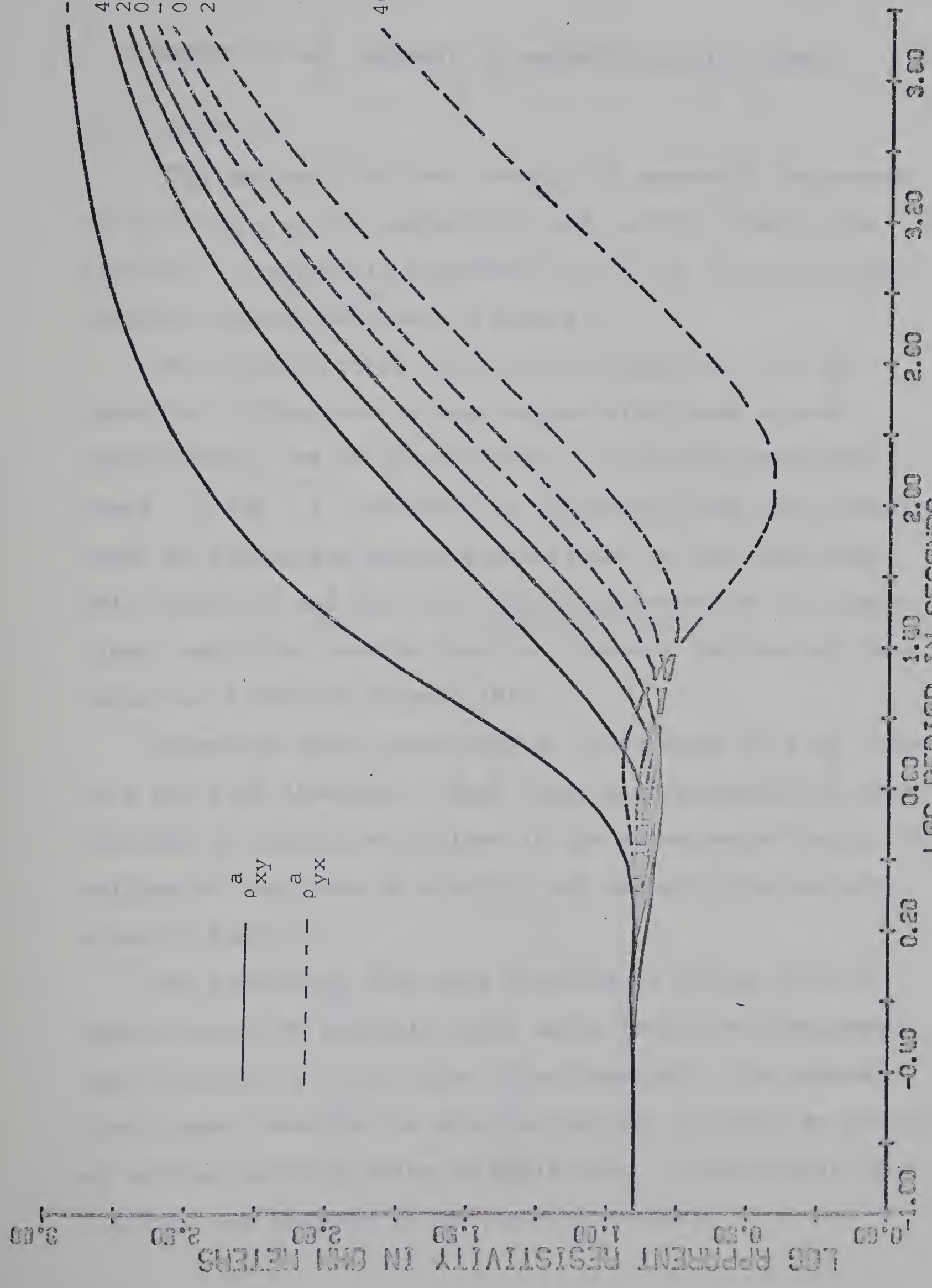

Figure 8: Computed apparent resistivity curves for four layered anisotropic earth model (Figure 6)

CHAPTER 3

DETECTION AND ANALYSIS OF MAGNETOTELLURIC SIGNALS

3.1. Detection

The geographical north-south and east-west components of variations in the geomagnetic and telluric fields are recorded. A schematic representation of the magnetotelluric recording system is shown in Figure 9.

The telluric field variations are derived from the potential differences between copper electrodes spaced approximately 500 ft (north-south) and 340 ft (east-west) apart. A 100 μf capacitor is introduced into the circuit to block DC potentials due to polarization at the electrodes. This capacitor and the total input resistance to the operational amplifier summing junction produces the desired lead corner at 0.0073 Hx (Figure 10).

Induction coils consisting of 32000 turns of wire, wound on a one inch diameter, 5 feet long, high permeability core are used to measure variations in the geomagnetic field. The calibrated responses of electric and magnetic systems are shown in Figure 10.

The recordings have been obtained in analog form on seven channel FM magnetic tapes using Precision Instruments tape recorder, at 15/16 ips. Simultaneously six channel brush paper recording is also carried out in order to provide an editing facility prior to digitizing. Time signals from W.W.V.B. are recorded on the seventh channel.

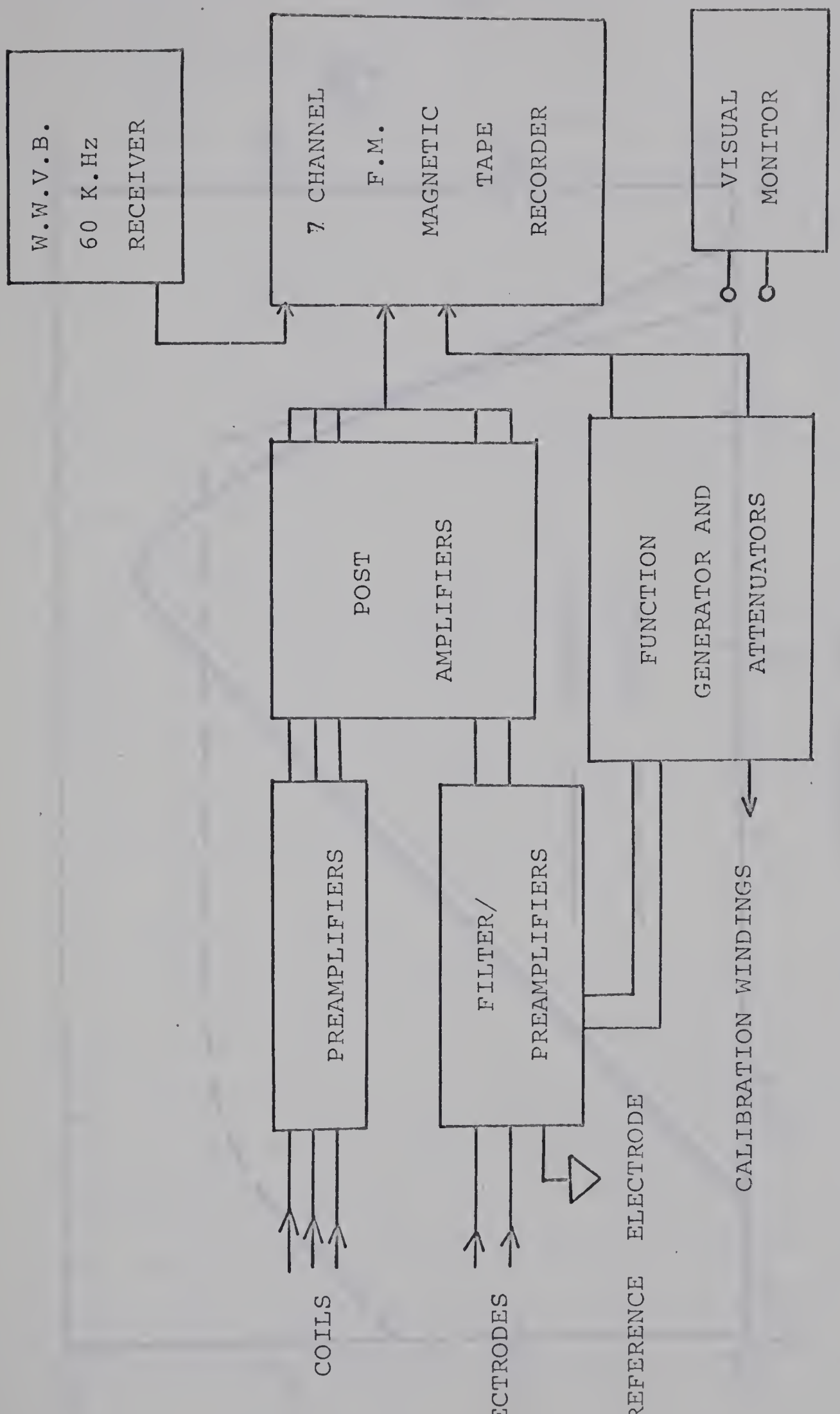

Figure 9: Block diagram of magnetotelluric recording system

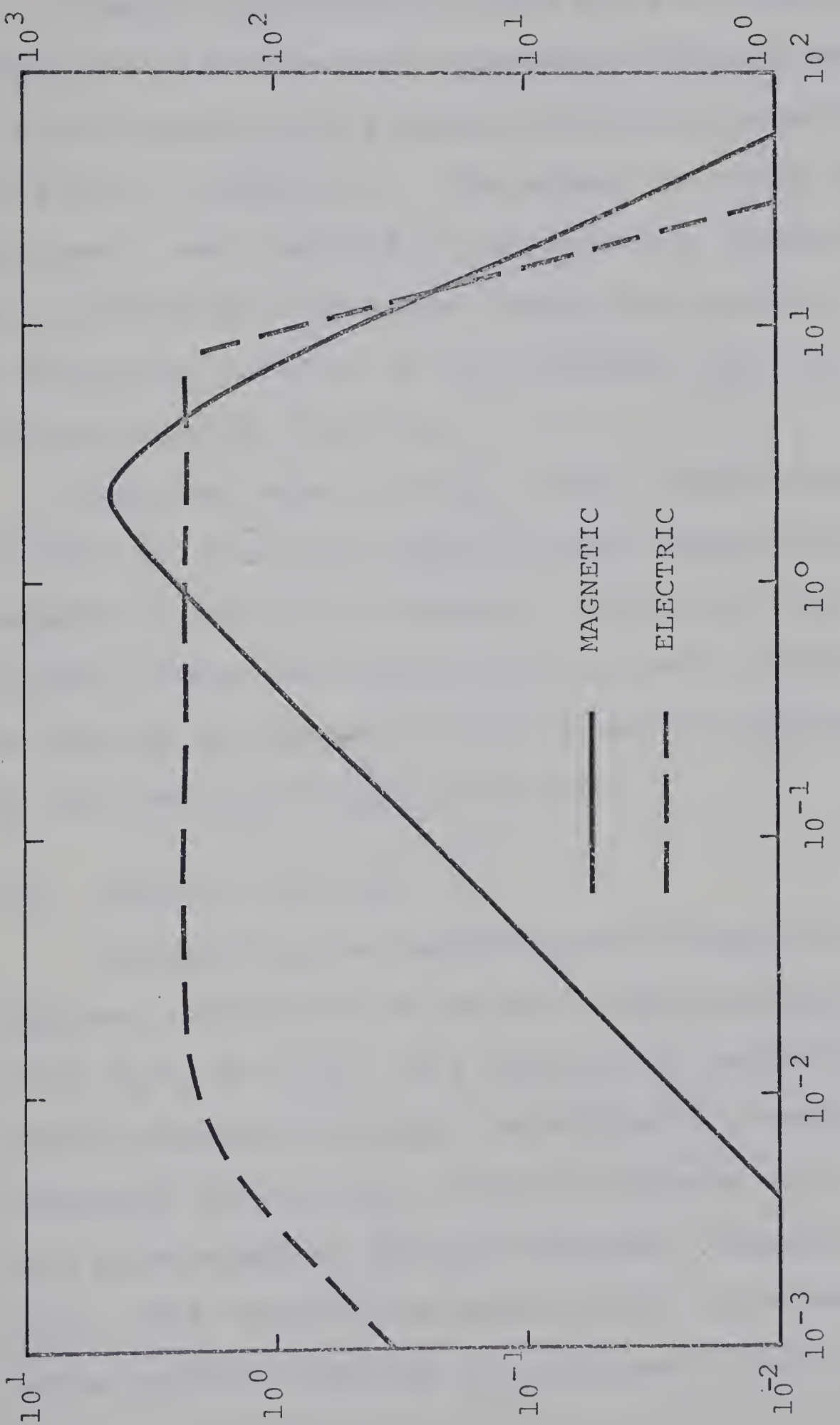

Figure 10: Calibrated responses of the electric and magnetic systems

3.2. Digital Processing

Records approximately three hours in length and free from discontinuities are selected for digital conversion. A block diagram of the Analog to Digital Conversion system is given in Figure 11. The signal in analog form is alias filtered and sampled by the Analog to Digital Converter at a rate of 15 samples per second per channel. This gives a digitizing interval of 32/15 seconds, with Nyquist frequency of approximately 0.25 Hz.

Digitized data in 11 bit binary form are recorded in blocks of 1200 two character words on seven channel asynchronous Kennedy digital tape recorders. Blocks are read alternately in each of the two output tape recorders (Figure 11) in order to provide the necessary Inter Record Gap required for input to the IBM 360/67 digital computer.

3.3. Spectral Analysis

In applying the magnetotelluric method to compute the apparent resistivity of the earth from Equation (2.12), the ratio E_x/H_y or E_y/H_x as a function of period (or frequency) can be obtained by visual inspection of a number of clear sinusoids (Berdchevskii, 1960; Srivastava et al., 1963) or from power spectral density estimates (Cantwell, 1960; Ellis, 1964; Hopkins and Smith, 1966; and others). The latter method is adopted in the present studies.

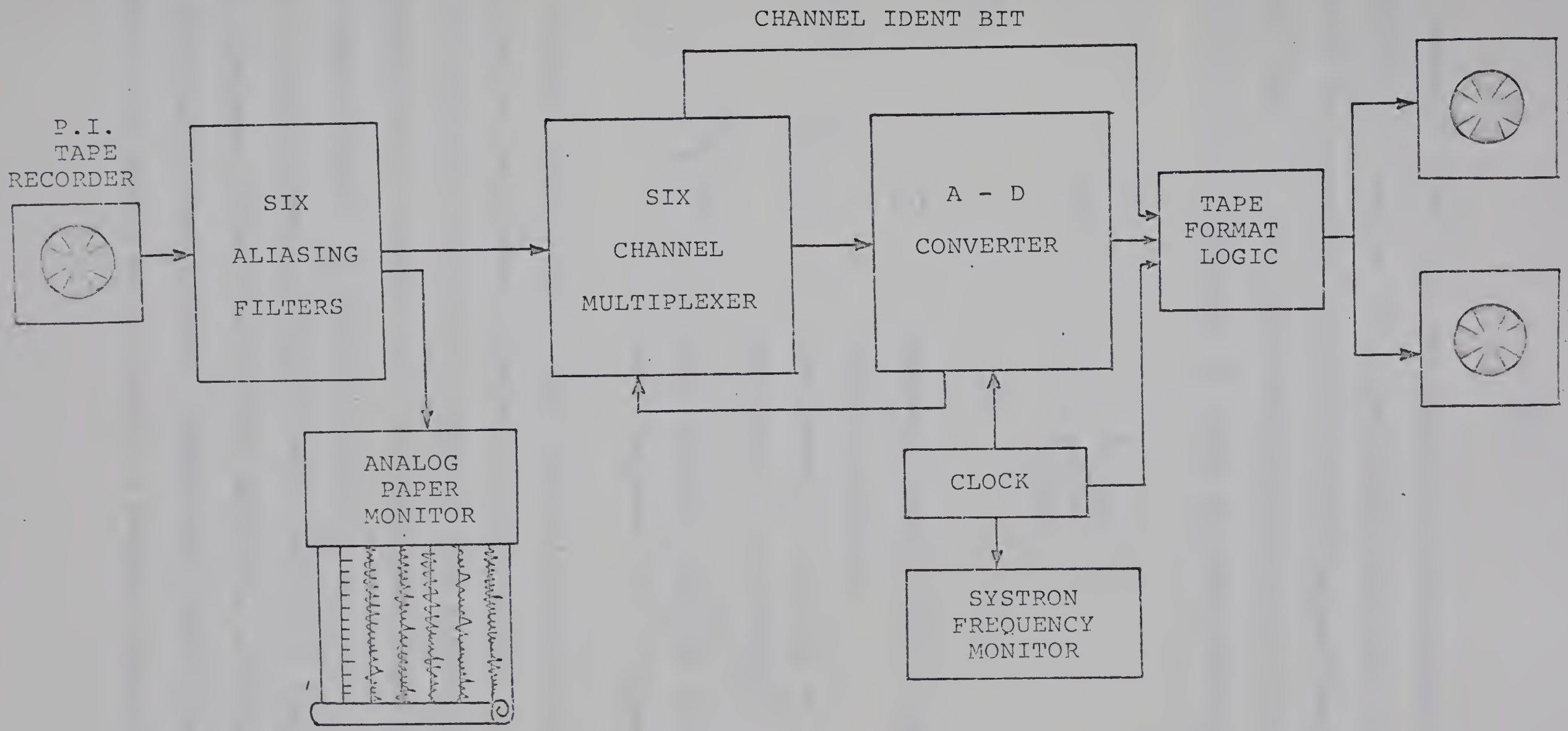

Figure 11: Block diagram of Analog to Digital Conversion system

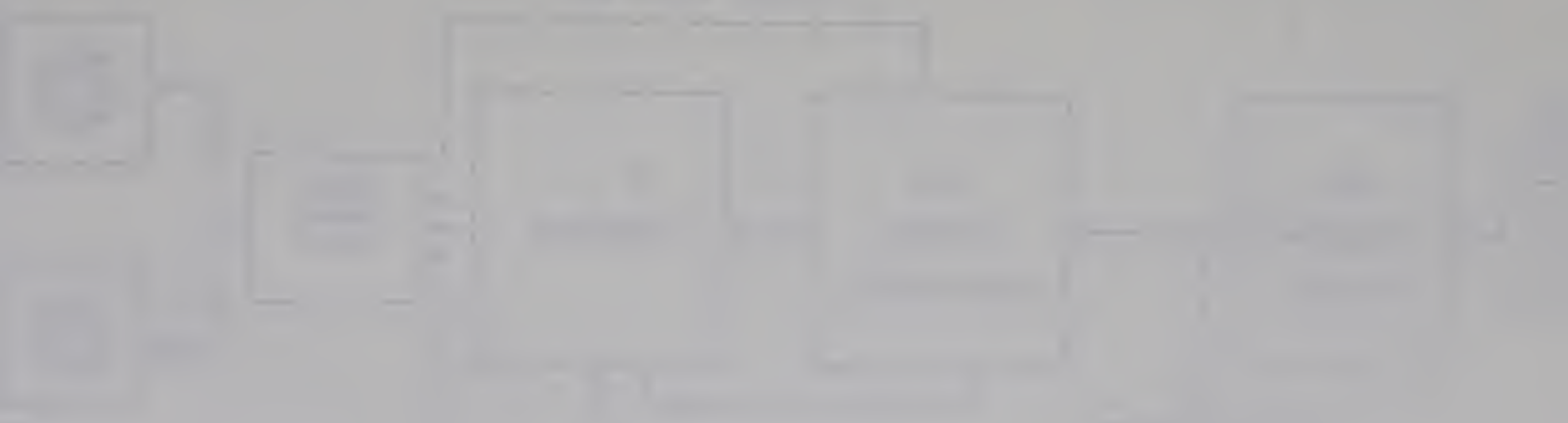

Cantwell (1960) has considered the magnetotelluric field components as samples of a stationary stochastic process and applied the numerical methods of Blackman and Tukey (1958) to the data. He has also shown that Equation (2.12) of Cagniard may be expressed in terms of power density spectra, as

$$\rho^a = 0.2\ T\ \frac{P_{E_x}(f)}{P_{H_y}(f)} \qquad (3.1)$$

where

ρ^a = apparent resistivity in ohm meters

T = period in seconds

$P_{E_x}(f)$ = power spectral density of telluric field component E_x in $(mv/km)^2 Hz$

$P_{H_y}(f)$ = power spectral density of the geomagnetic field component H_y in $(gammas)^2/Hz$.

A brief description of the spectral computational technique employed in the present studies is given below.

The spectral analysis is based on the assumption that magnetotelluric records are from stationary processes with zero mean values. If the mean value is not zero, then the power spectral density function will exhibit a large peak at zero frequency which will distort estimates at other frequencies. For this reason the original records are conditioned by subtracting the sample mean values. A second correction is

applied to correct for the slowly varying linear trend (that is, non zero slope with respect to time). This may be due to instrumentation drift or to an actual underlying linear trend in the data, such as diurnal variations.

If $x(t)$ is the original series of length R_1, the corrected series $\bar{x}(t)$ is written according to Bendat and Piersol (1966), as

$$\bar{x}(t) = x(t) - x_m - \alpha_x \left(t - \frac{R_1}{2}\right) \qquad (3.2)$$

$$0 \leq t \leq R_1$$

where

$$x_m = \frac{1}{N} \sum_{i=1}^{N} x_i \qquad (3.3)$$

denotes the sample mean value of $x(t)$ over $(0, R_1)$, the parameter α_x denotes the average slope,

$$\alpha_x = \frac{1}{\nu(N-\nu)} \left| \sum_{n=N-\nu}^{N} x_n - \sum_{n=1}^{\nu} x_n \right| \qquad (3.4)$$

where N is the total number of data samples and ν is the largest integer less than or equal to N/3.

The Fast Fourier Transform (FFT) algorithm of Cooley and Tukey (1965) (Appendix 2) is used to compute the covariance functions and spectral density estimates.

The Discrete Fourier Transform (DFT) of a series x(t) is defined as

$$X(W) = \sum_{t=0}^{N-1} x(t) \; e^{\frac{-2 \pi i t W}{N}}$$

$$W = 0, 1, 2 \ldots N - 1 \quad (3.5)$$

where W is the digital frequency index and N is the total number of data points.

Covariance functions are obtained employing the convolution theorem techniques of Sande (1965) rather than summing the lagged products which is computationally expensive. For example, the autocovariance function of the series x(t) is given by

$$a(\tau) = \frac{1}{N'} \left[\sum_{W=0}^{N'-1} \left\{ X^*(W) \; X(W) \right\}^* \quad e^{\frac{-2 \pi i W \tau}{N'}} \right]^* \quad (3.6)$$

where τ is the lag number, N' is the total number of points including zeros added to the series x(t) to maintain the cyclic nature of the data, X(W) is the DFT of x(t) as defined in Equation (3.5) and * represents the complex conjugate.

The raw covariance functions thus obtained are smoothed using the lag window of Parzen (1961) with the weighing coefficients

$$W(\tau) = 1 - 6\left(\frac{\tau}{m}\right)^2 + 6\left(\frac{\tau}{m}\right)^3, \quad \tau < \frac{M}{2}$$

$$= 2\left[1 - \left(\frac{\tau}{m}\right)\right]^3, \quad \frac{M}{2} < \tau < M$$

$$= 0 \qquad \tau > M \qquad (3.7)$$

where M is the maximum number of lags. The Parzen lag window has proved to be more efficient for magnetotelluric analysis. It involves less computational effort than, for example, the Daniel window, at the same time giving positive power estimates with extremely low side lobes, and further, it keeps the sample coherence between its theoretical limits ± 1.

The power density spectra are obtained by taking the Fourier transforms of the smoother covariance functions. The autopower density spectrum of the x(t) series is thus given by

$$P_x(W) = \sum_{\tau = 0}^{M = 1} a_m(\tau) \; e^{\frac{-2 \pi i W \tau}{M}} \qquad (3.8)$$

where $a_m(\tau)$ is the smoothed (or modified) value of $a(\tau)$ in Equation (3.6).

The crosscovariance function of x(t) and y(t) series is defined as the Fourier transform of the product X*(W) Y(W),

$$c(\tau) = \frac{1}{N'}\left[\sum_{W = 0}^{N' - 1} \left\{ X^*(W)\; Y(W) \right\}^* \; e^{\frac{-2 \pi i W \tau}{N'}}\right]^* \qquad (3.9)$$

where Y(W) is the DFT of the y(t) series and the rest of the notation is the same as in Equation (3.6). The crosspower density spectrum is then obtained by taking the Fourier transform of the smoothed crosscovariance function.

The sample coherence between orthogonal electric and magnetic field components is also computed using the definition

$$\gamma(f) = \frac{|P_{xy}(f)|}{\sqrt{P_x(f)\ P_y(f)}} \qquad (3.10)$$

where

$\gamma(f)$ = sample coherence

$P_{xy}(f)$ = crosspower density spectrum

$P_x(f), P_y(f)$ = autopower density spectra of x and y series

Examples of the autopower density spectra of orthogonal electric and magnetic field components and the sample coherence between them are given in Figures 12 and 13. The number of points and the maximum number lag used were 4096 and 512 respectively.

If the spectral density estimates at a frequency f_o are to be useful, only frequencies close to f_o should have substantial contribution. If the spectrum rises steeply as f leaves f_o, an extremely rapid fall-off in the spectral window is required. To avoid this problem Blackman and Tukey (1958), Ellis (1964) and others have recommended the pre-whitening of the data before computing the spectrum.

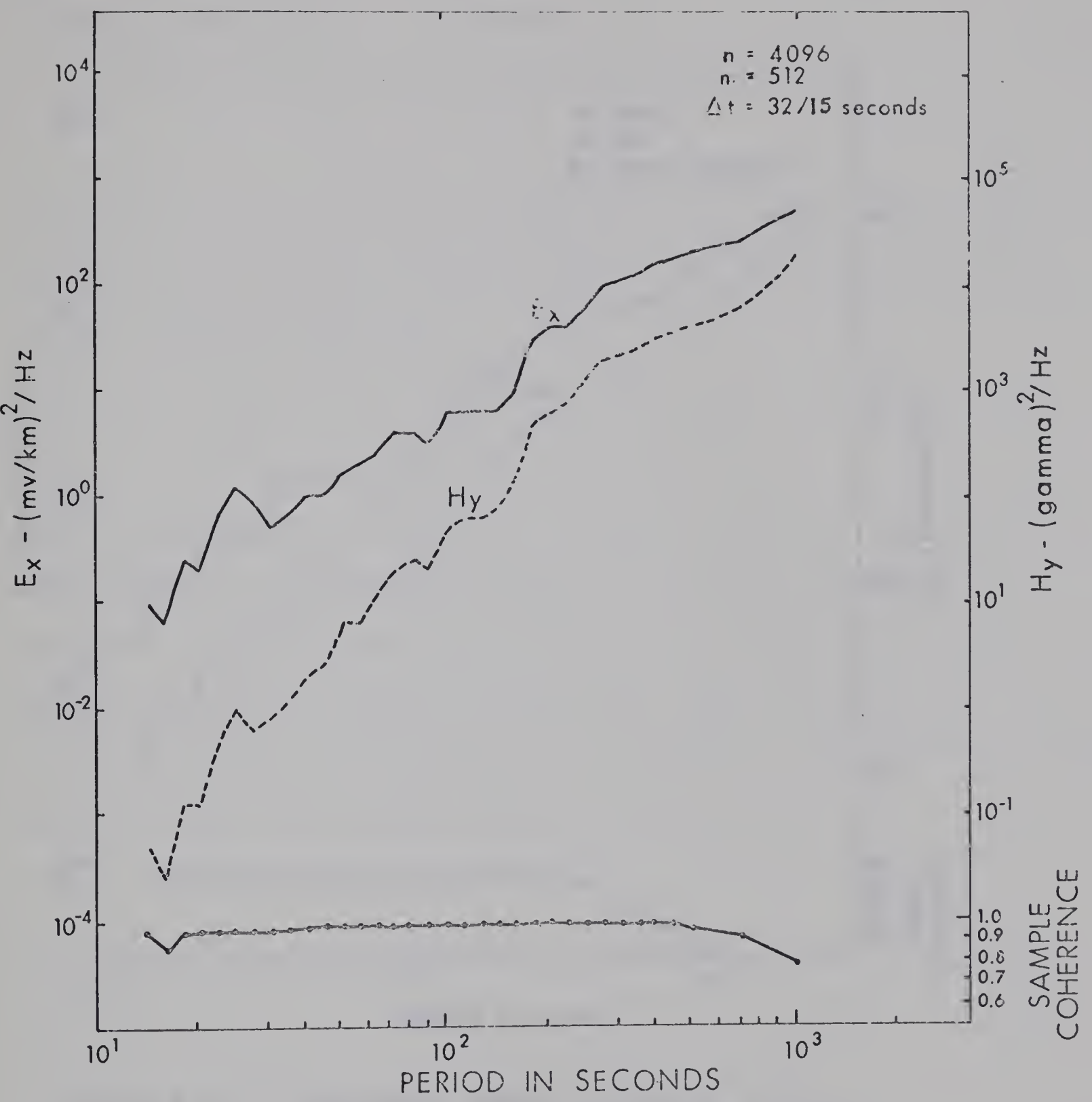

Figure 12: Autopower density spectra of E_x (north-south electric) and H_y (east-west magnetic) and the sample coherence between them

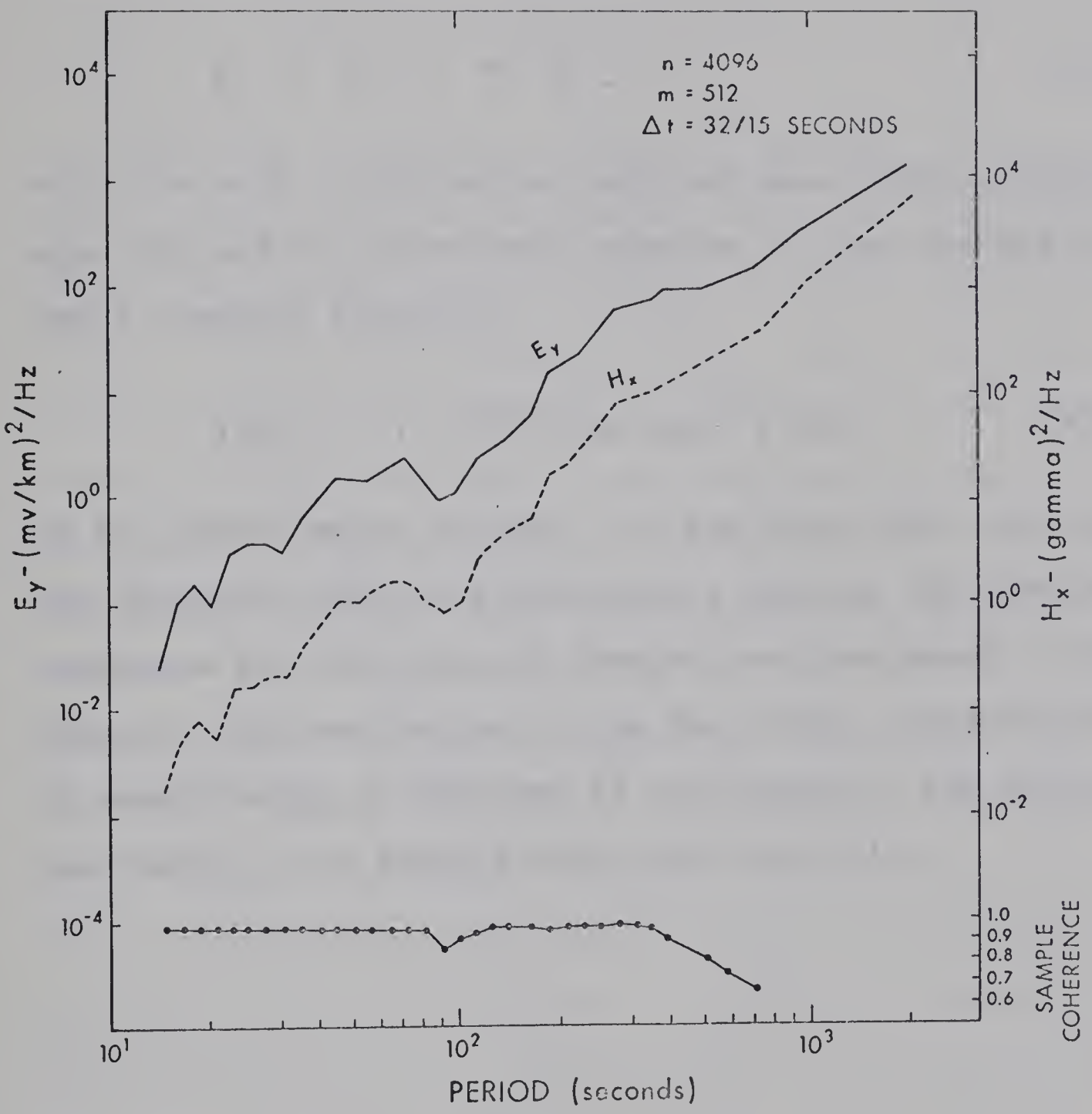

Figure 13: Autopower density spectra of E_y (east-west electric) and H_x (north-south magnetic) and the sample coherence between them

In order to test the whiteness of the present data, a prewhitening filter of the form

$$z_i = x_i + K\ x_{i-1} \tag{3.11}$$

with K = -0.9 is applied to original data before computing the spectrum and the calculated spectrum is then divided by the power transfer function,

$$Y(f) = (1 + K^2 + 2K \cos 2\pi f\Delta t), \tag{3.12}$$

of the prewhitening process. It was found that this prewhitening operation did not significantly improve the spectral estimates for the range of frequencies considered in this thesis. This may be due to the fact that a considerable amount of prewhitening is achieved in the design of the recording system and further, the spectra were relatively flat.

CHAPTER 4

RESULTS AND INTERPRETATION

Apparent resistivity curves ρ^a_{xy} and ρ^a_{yx} in the north-south and east-west directions respectively, were obtained following the power spectrum analysis methods outlined in Chapter 3, and using Equation (3.1). Spectral density estimates, for which the sample coherence between orthogonal electric and magnetic field components was greater than 0.9, were used to compute apparent resistivities ρ^a_{xy} and ρ^a_{yx}. The average apparent resistivity values thus obtained from 20 "good" data sets, recorded on different days and times at the University of Alberta Geophysical Observatory, are plotted as functions of period in Figure 14. The error bars in the figure correspond to maximum deviation from the mean. These apparent resistivity curves deviate significantly for periods greater than 20 seconds, suggesting a strong anisotropy at the measuring site. Similar types of anisotropy are reported by Fournier (1962) at Garchy, Nivre in France, and by Hopkins and Smith (1966) at Pecos, Texas.

Polarization studies have also been made for all data sets chosen for the analysis. Plots of the electric and magnetic field polarization values are line printed directly from the computer and are illustrated in Figures 15 and 16. These plots which are typical of all the data sets are each

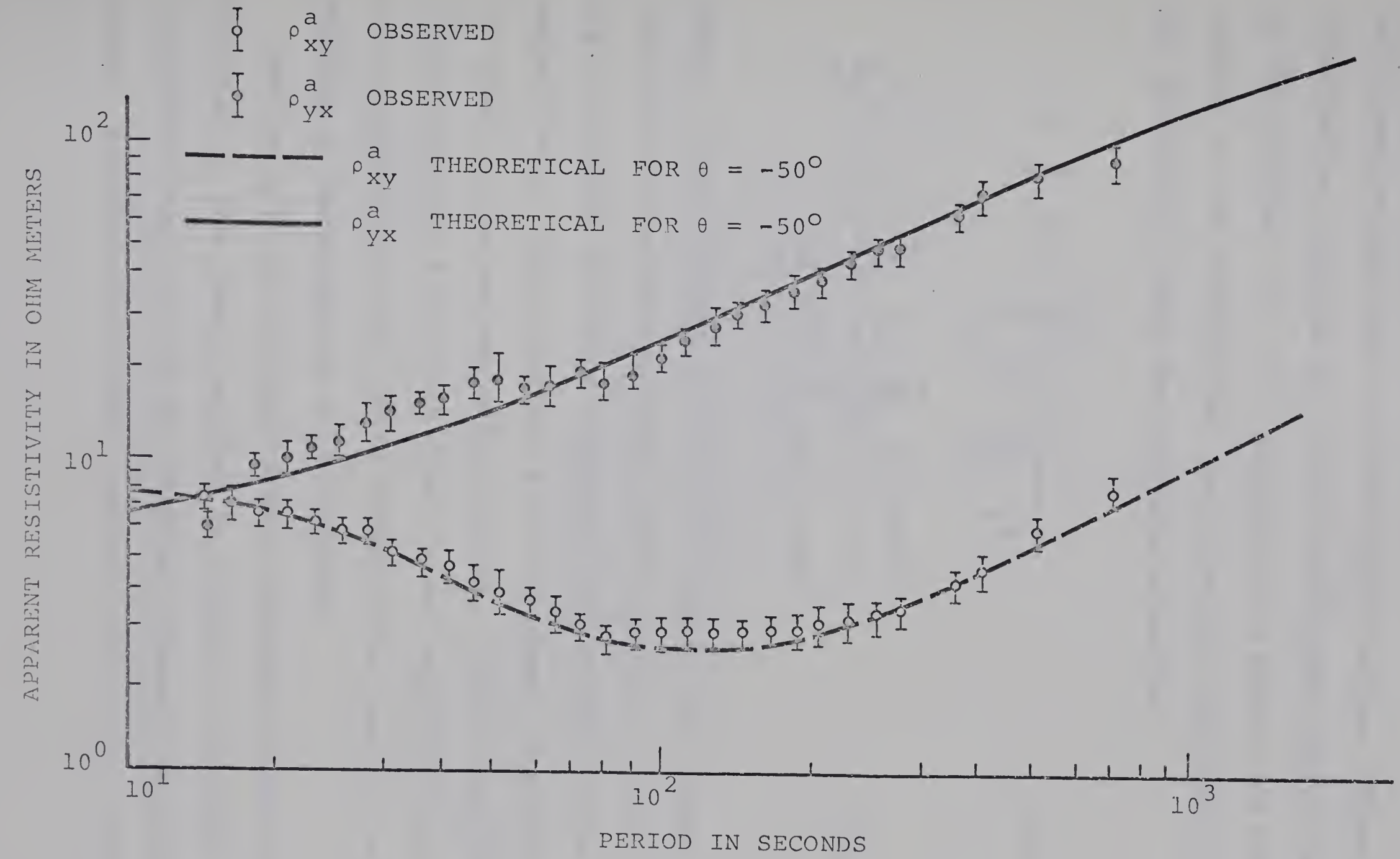

Figure 14: Apparent resistivity curves at the University of Alberta Geophysical Observatory and the computed apparent resistivity curves for the model shown in Figure 17

calculated on the basis of 3600 digital values. These polarization diagrams are fitted to ellipses and the parameters of the ellipses viz., the azimuth of the major axis with respect to the geographical north (X-axis) and the ellipticity are obtained by using the following equations

$$\alpha = \frac{1}{2} \tan \frac{2 \sum_{i=1}^{n} x_i y_i}{\sum_{i=1}^{n} x_i^2 - \sum_{i=1}^{n} y_i^2} \qquad (4.1)$$

$$\frac{b^2}{a^2} = \frac{1 - (\sum_{i=1}^{n} x_i^2 / \sum_{i=1}^{n} y_{i)}^2 \tan^2\alpha}{(\sum_{i=1}^{n} x_i^2 / \sum_{i=1}^{n} y_i^2) - \tan^2\alpha} \qquad (4.2)$$

where α is the azimuth of the major axis of the ellipse measured in clockwise direction with respect to North, and a and b represent the major and minor axes of the ellipse respectively. The parameters of the ellipses thus obtained are given in the corresponding figures. The non-orthogonality of the resultant horizontal electric and magnetic fields for the Pc_4 type pulsations, which dominate the results, is further evidence of anisotropy at this location.

Various anisotropic earth models (Appendix 3) were considered, according to the theory outlined in Chapter 2, in order to get a resonably good fit with the observed apparent resistivity curves. A model which yields apparent resistivity curves

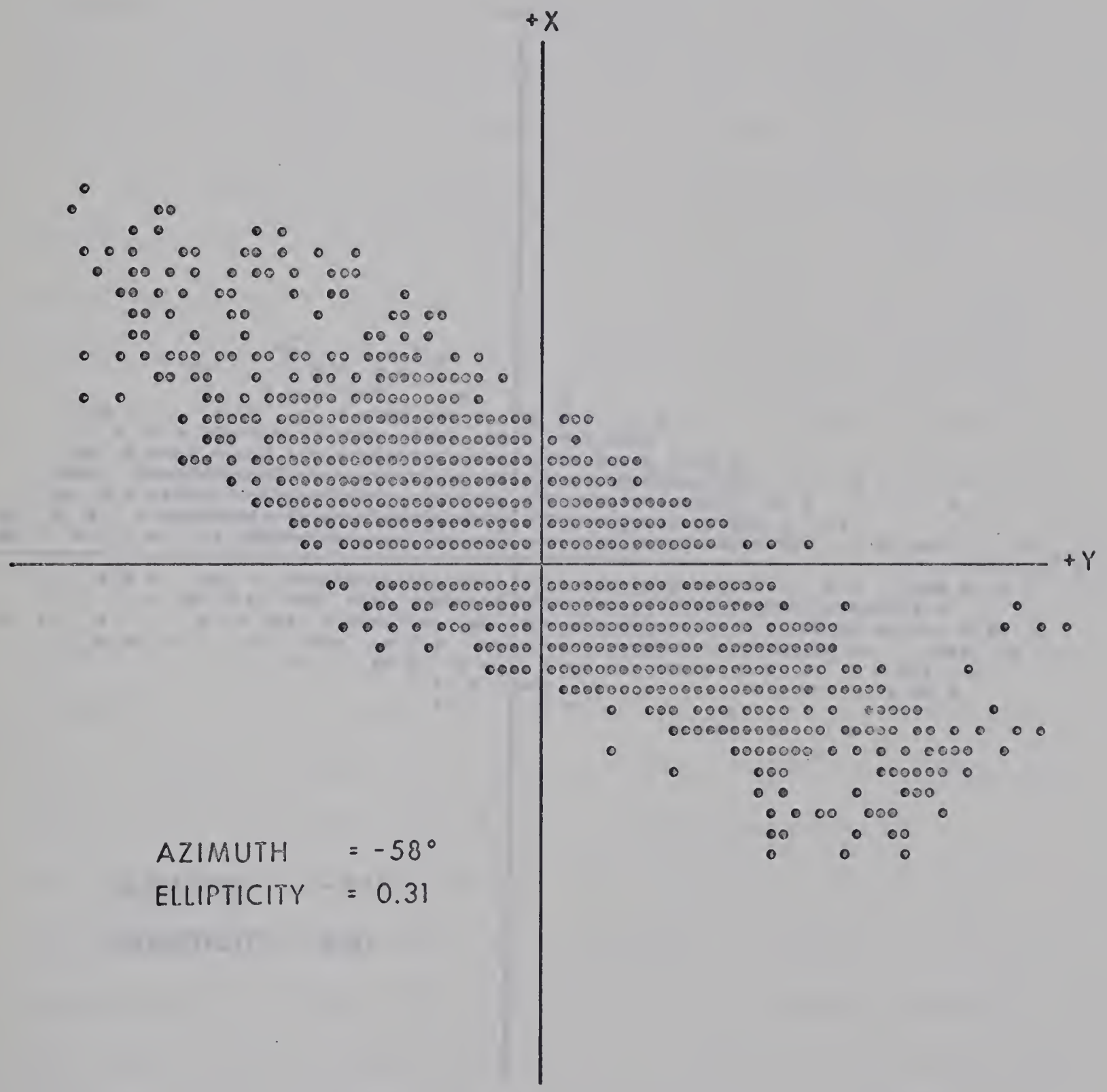

Figure 15: Electric field polarization

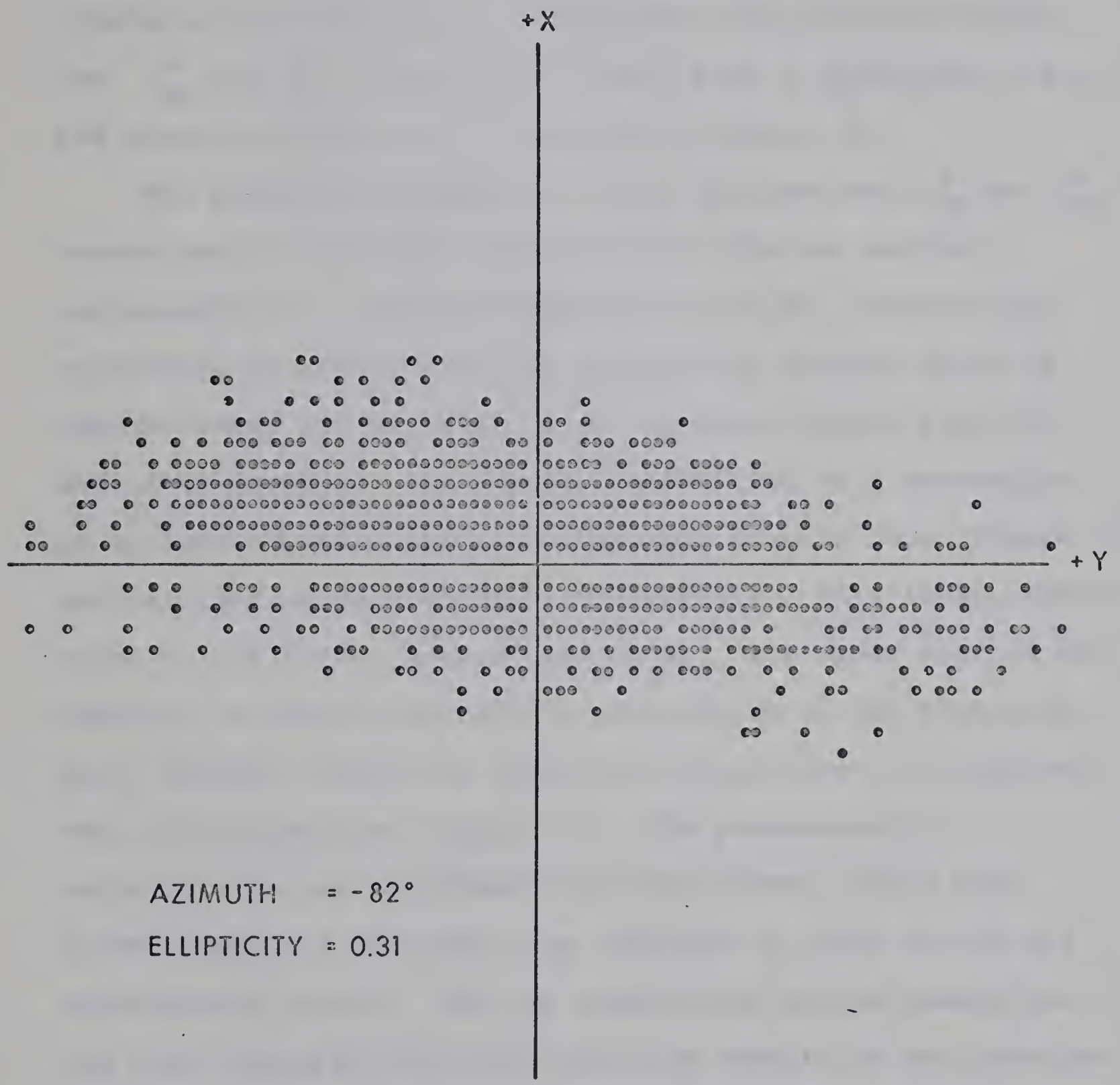

Figure 16: Magnetic field polarization

which are in close agreement with observations, is shown in Figure 17. A set of resistivity curves obtained for the model given in Figure 17, is shown in Figure 18 for various values of θ, the angle from the major axis of anisotropy in clockwise direction to the north-south axis of measurement. The ρ^a_{xy} and ρ^a_{yx} curves for $\theta = -50^o$ give a reasonable fit to the observed curves as illustrated in Figure 14.

The period 20 seconds, at which the observed ρ^a_{xy} and ρ^a_{yx} curves start to deviate significantly from one another, corresponds to a depth of approximately 6 km. Thus it is reasonable to assume that the sedimentary section which is approximately 2.5 km thick is an isotropic single layer for modelling purposes. An average resistivity of 8 ohm-meters is assigned to this layer on the basis of well logs (Figure 1) and previous magnetotelluric measurements. This layer corresponds to the first layer of the model. The upper part of the basement is mainly gneissic in composition at the measuring site, however, there are significant variations in lithology over short distances (Figure 2). The parameters viz., resistivities and thicknesses for the second, third and fourth layers of the model are selected in order to fit the experimental curves. The low resistivity values chosen for the third layer do not agree with the results of the previous workers, except for the result by Vozoff et al. (1963) at Kavanagh for which they did not attempt an interpretation. The apparent resistivity curves obtained by them for the

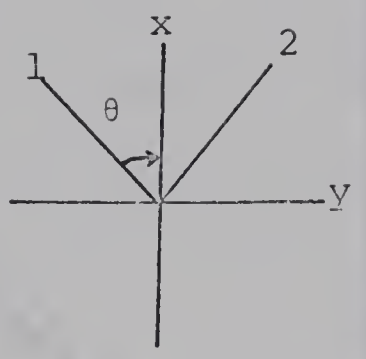

	Depth (km)
$\rho_1 = \rho_2 = 8\ \Omega$ m	2.5
$\rho_1 = 400\ \Omega$ m, $\rho_2 = 200\ \Omega$ m	4.5
$\rho_1 = 40\ \Omega$ m, $\rho_2 = 10\ \Omega$ m	12.5
$\rho_1 = \rho_2 = 1000\ \Omega$ m	

Figure 17: Four layered anisotropic earth model

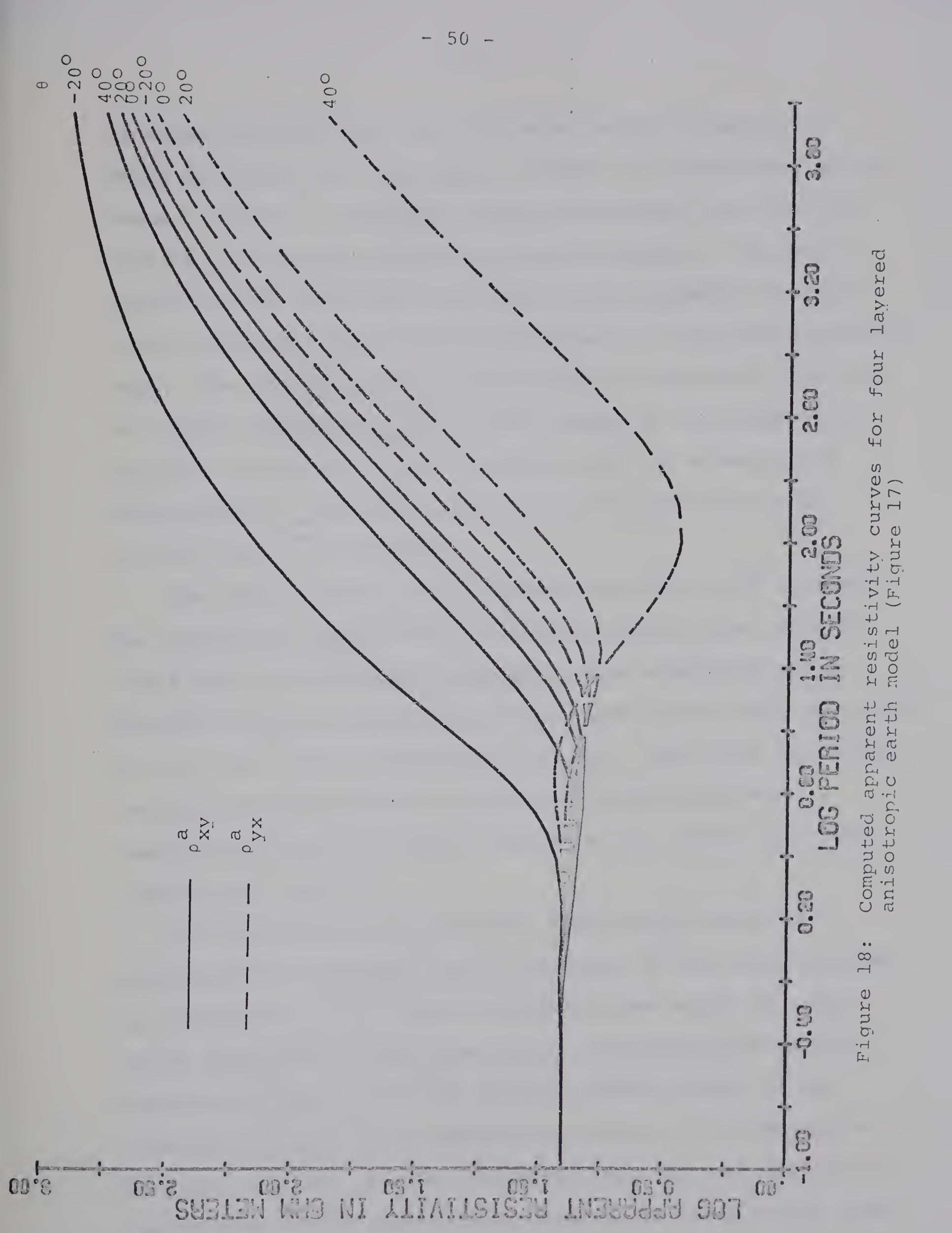

Figure 18: Computed apparent resistivity curves for four layered anisotropic earth model (Figure 17)

Kavanagh station, which is a few miles south of Leduc, are shown in Figure 19. The depth to which the lithological units, shown in Figure 2, extended within the basement was given by Garland and Burwash (1959) from gravity studies. The depth quoted by them was 8 km, which is in good agreement with the total thickness of the anisotropic layers in the model presented here. The 1000 ohm meters resistivity of the bottom layer can be varied considerably with little change in the shape of the apparent resistivity curves, however, only an extension of measurements at the long period end of the spectrum could provide conclusive results.

The major direction of anisotropy which is N 50° E cannot be interpreted unambiguously with the present state of knowledge about the basement structure. This anisotropy may be related to major geologic structures such as the Rocky Mountains or to a more local conductivity anomaly. The effect of distant vertical discontinuities on measured surface apparent resistivity has been shown by Rankin et al. (1965) from their analog model studies.

The direction of the electric field vector which is predominantly polarized N 58° W is close to the value obtained by Srivastava et al. (1963) at Cooking Lake which is a few miles north-east of the Observatory. They interpreted this north-west direction of the electric vector as due to the structural trends in the sedimentary layers. An examination of analog records, however indicates that the contribution to the electric field polarization (Figure 15) comes mainly from

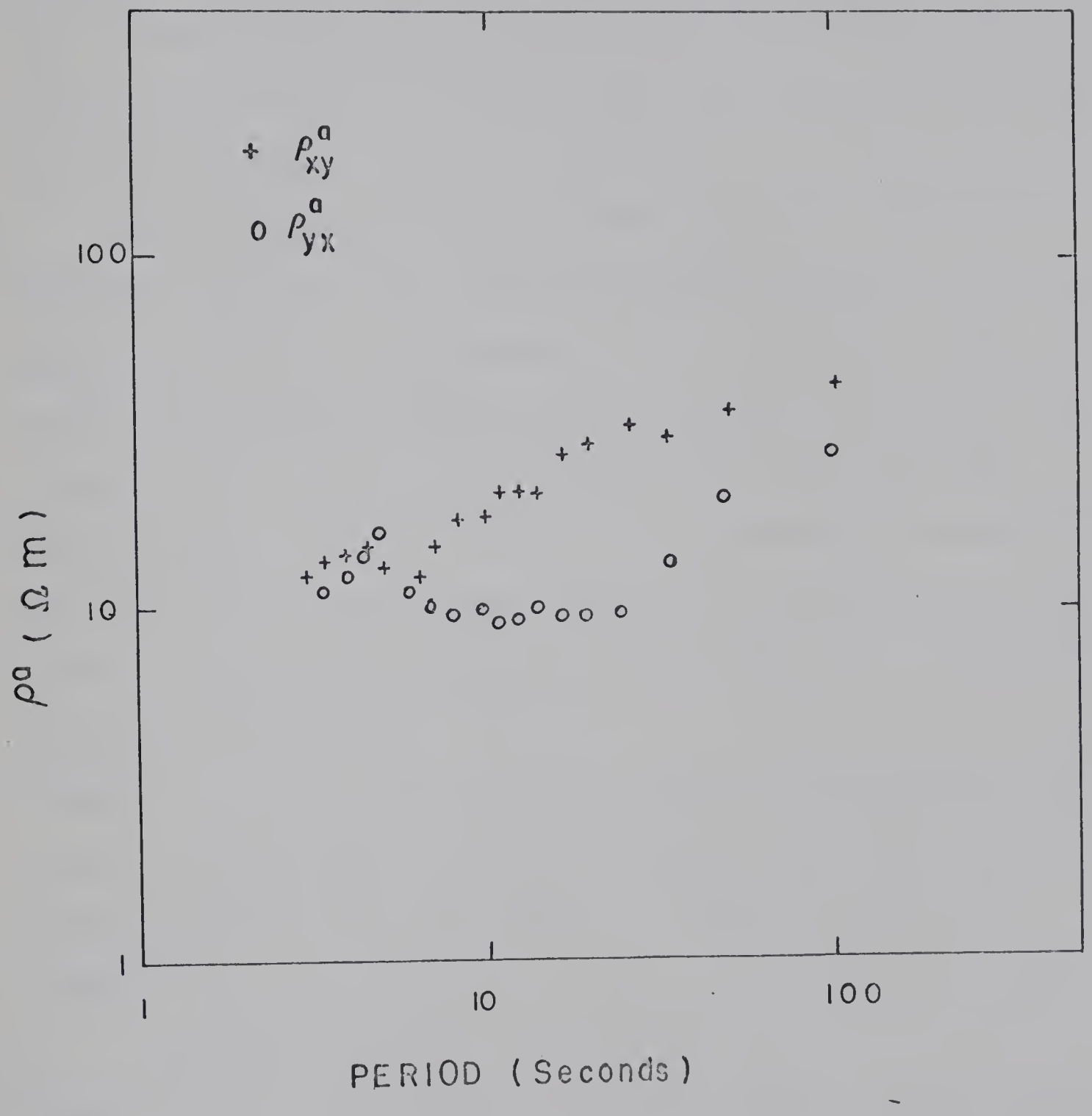

Figure 19: Apparent resistivity curves at Kavanagh, Alberta (after Vozoff et al. 1963)

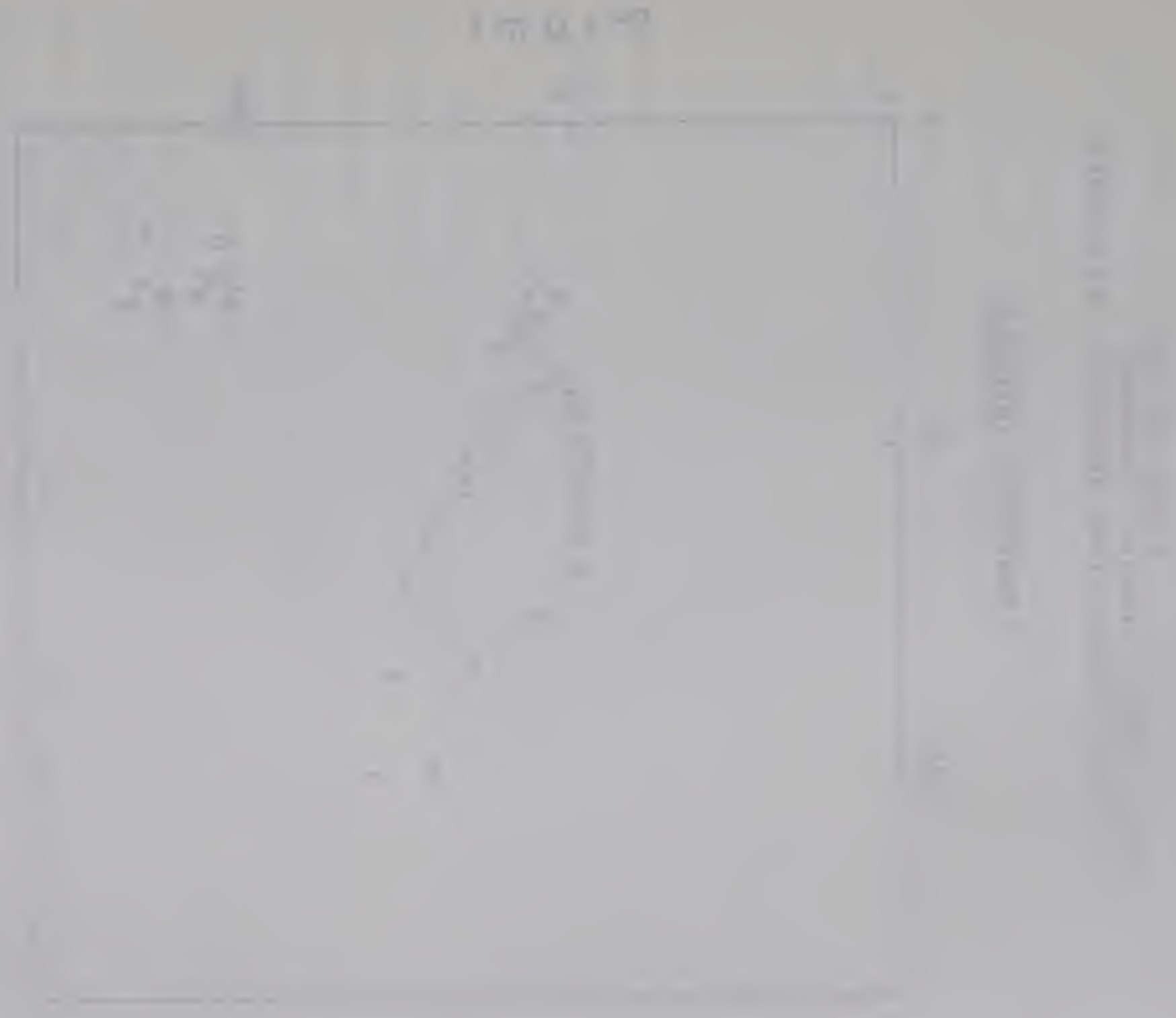

the periods ranging from 60 to 150 seconds, which have much deeper penetration.

CONCLUSIONS AND SUGGESTIONS FOR FURTHER WORK

From the apparent resistivity curves presented in this thesis, it may be seen that employing refined instrumentation and "good" statistics reduces the scatter in the apparent resistivity curves to a level such that reliable comparison can be made with model calculations.

While neither crustal seismic data nor aeromagnetic data are available for this particular location, a pronounced directional trend is noticeable along the direction of the major axis of anisotropy in the aeromagnetic map* of the Cooking Lake area, which is a few miles North of the Observatory. In order to make a satisfactory interpretation of the apparent anisotropy observed at the Observatory a close spaced magnetotelluric network with other geophysical coverage is necessary. Further, an analysis of the vertical component of the magnetic field and the determination of phase relationships between horizontal electric and magnetic field components may be helpful in interpreting this resistivity anisotropy.

Care must be taken to avoid the problem of measuring field components in the direction of polarization. This can be done by reconnaissance survey in order to determine the appropriate direction for the sensors or by recording two orthogonal components at various orientations.

* Geophysics paper 33, G.S.C., OTTAWA, 1951.

REFERENCES

Bendat, J.S., A.G. Piersol, Measurement and Analysis of Random Data, John Wiley & Sons, Inc., New York, 1966.

Berdichevskii, M.N., Electrical Prospecting with the Telluric Current Method, Gostoptekhizdot, Moscow, 1960. (English translation by Keller, G.V., Quarterly of the Colorado School of Mines, 60, 1, 1965).

Bingham, C., M.D. Godfrey and J.W. Tukey, Modern techniques of power spectrum estimation. IEEE Transaction on Audio and Electroacoustics, AU-15, 56-66, 1967.

Blackman, R.B., and J.W. Tukey, The Measurement of Power Spectra, Dover Publications, New York, 1958.

Bostick, F.X., Jr., and H.W. Smith, Investigation of large-scale inhomogeneities in the earth by the magne-totelluric method, Proc. IRE, 50, 2339-2346, 1962.

Cagniard, L., Basic theory of the magnetotelluric method of geophysical prospecting, Geophysics, 18, 605-635, 1953.

Cantwell, T., Detection and anlysis of low frequency magne-totelluric signals, Ph.D. thesis, Department of Geology and Geophysics, Massachusetts Institute of Technology, 1960.

Chetaev, D.N., The determination of anisotropy coefficient and the angle of inclination of homogeneous aniso-tropic medium, by measuring the impedance of natural electromagnetic field, Bull. Acad. Sci. USSR, Geophysics ser., English Transl., 407-408, 1960.

Cooley, J.W., and J.W. Tukey, An algorithm for the machine calculations of Complex Fourier Series, Mathematics of Computation, 19, 297-307, 1965.

Cooley, J.W., P.A.W. Lewis, and P.D. Welch, Historical notes on the Fast Fourier Transform, IEEE Transactions on Audio and Electroacoustics, AU-15, 75-79, 1967.

Danielson, G.G., and C. Lanczos, Some improvements in practical Fourier analysis and their application to X-ray scattering from liquids. J. Franklin Inst., 233, 365-380 and 435-452, 1942.

d'Erceville, I., and G. Kunetz, The effect of a fault on the earth's natural electromagnetic field, Geophysics, 27, 651-665, 1962.

Dosso, H.W., Analogue model measurements for electromagnetic variations near faults and dykes, Can. J. of Earth Sciences, 3, 287-303, 1966.

Ellis, R.M., Analysis of natural ultra low frequency electromagnetic fields, Ph.D. thesis, Department of Physics, University of Alberta, 1964.

Fournier, H.G., Directional magnetotelluric spectra at Garchy, Nivre, Ann. de Geophy. 19, 138-148.

Garland, G.D., and R.A. Burwash, Geophysical and petrological study of Precambrian of central Alberta, Bull Am. Assoc. Petrol. Geologists, 43, 790-806, 1959.

Gentleman, W.M. and G. Sande, Fast Fourier transform for fun and profit, 1966. Fall Joint Computer Conf., AFIPS Proc., 29, 563-578, 1966.

Hopkins, A.H. and H.W. Smith, An investigation of magnetotelluric method for determining subsurface resistivities. Report No. 140, EERL., University of Texas, 1966.

Jones, D.S, The theory of Electromagnetism, The Macmillan Company, New York, 1964.

Kato, Y., and T. Kikuchi, On the phase difference of earth currents induced by the changes of the earth's magnetic field, Parts I and II, Science Reports of Tohoku University, Series 5, Geophysics, 2, 139-145, 1950.

Kovtun, A.A., The magnetotelluric investigation of structures inhomogeneous in layers, Bull. Acad. Sci. USSR, Geophys. ser., English transl., 1085-1087, 1961.

Madden, T., and P. Nelson, A defence of Cagniard's magnetotelluric method, Project NR-371-401, Geophysics Laboratory, Massachusetts Institute of Technology, 1964.

Mann, J.E., Magnetotelluric theory of sinusoidal interface, J. Geophys. Res., 69, 3527-3524, 1964.

Mann, J.E., The importance of anisotropic conductivity in magnetotelluric interpretation, J. Geophys. Res., 70, 2940-2942, 1965.

Neves, A.S., The magnetotelluric method in two-dimensional structures, Ph.D. thesis, Department of Geology and Geophysics, Massachusetts Institute of Technology, 1957.

O'Brien, D.P., and H.F. Morrison, Electromagnetic fields in an n-layer anisotropic half-space, Geophysics, 32, 668-677, 1967.

Parzen, E., Mathematical considerations in the estimation of spectra, Technometrics, 3, 167-189, 1961.

Price, A.T., The theory of the magnetotelluric method when the source field is considered, J. Geophys. Res., 67, 1907-1918, 1962.

Rankin, D., The magnetotelluric effect on a dyke, Geophysics, 27, 666-676, 1962.

Rankin, D., G.D. Garland and K. Vozoff, An analog model for the magnetotelluric effect, J. Geophys. Res., 70, 1939-1945, 1965.

Richards, T.D., and D.J. Walker, Measurement of the thickness of the earth's crust in the Albertan plains of Western Canada, Geophysics, 24, 262-284, 1959.

Rikitake, T., Electromagnetic induction within the earth and its relation to the electrical state of the earth's interior, Bull. Earthq. Res. Inst. Tokyo, 28, 45-98, 1950.

Rikitake, T., Changes in earth currents and their relation to the electrical state of the earth's crust. Bull. Earthq. Res. Inst. Tokyo, 29, 270-275, 1951.

Rokityanski, I.I., On the application of the magnetotelluric method to anisotropic and inhomogeneous masses. Bull. Acad. Sci. USSR, Geophys. Ser., English Transl. 1050-1053, 1961.

Sande, G., On an alternative method of calculating covariance functions, Unpublished manuscript of Princeton University, 1965.

Schelkunoff, S.A., Electromagnetic waves, D. Van Nostrand Co., New York, 1943.

Srivastava, S.P., J.L. Douglass and S.H. Ward, The application of magnetotelluric and telluric methods in central Alberta, Geophysics, 28, 998-1008, 1963.

Srivastava, S.P., Method of interpretation of magnetotelluric data when source field is considered. J. Geophys. Res. 70, 945-954, 1965.

Srivastava, S.P., Magnetotelluric two and three layer master curves, Publications of the Dominion Observatory, Ottawa, Volume 35, No. 7, 1967.

Swift, C.M. Jr., A magnetotelluric investigation of an electrical conductivity anomaly in the southwestern United States, Ph.D. thesis, Department of Geology and Geophysics, Massachusetts Institute of Technology, 1967.

Tikhonov, A.N., Determination of the electrical characteristics of deep layers of the earth's crust, Dok. Akad. Nauk., USSR, 73, 295-297, 1950.

Tikhonov, A.N. and M.N. Berdichevskii, Experience in the use of magnetotelluric methods to study the geologic structure of sedimentary basins, Bull. Acad. Sci., USSR, Earth Physics, English Translation, 93-97, 1966.

Vozoff, K., H. Hasegawa, and R.M. Ellis, Results and limitations of magnetotelluric surveys in simple geologic situations, Geophysics, 28, 778-792, 1963.

Wait, J.R., On the relation between telluric currents and the earth's magnetic field, Geophysics, 19, 281-285 1954.

Weaver, J.T., The elctromagnetic field within a discontinuous conductor with reference to geomagnetic micropulsations near a coast line, Can. J. Phys., 41, 484-495, 1963.

Welch, P.D., The use of the Fast Fourier transform for the estimation of power spectra: A method based on time averaging over short, modified periodograms, IEEE Transactions on Audio and Electroacoustics, AU-15, 70-79, 1967.

Wiese, H., Geomagnetische Tiefentellusik, Tiel I, Geofisica Pura E. Applicata, 51, 59-78, 1962.

Yungul, S., Magnetotelluric sounding three-layer interpretation curves. Geophysics, 26, 465-473, 1961.

APPENDICES

APPENDIX 1

A1.1. Anisotropic Half-Space

For a half-space whose conductivity is different in different directions, Ohm's law is written as

$$| \vec{J} | = | \sigma_{m,n} | | \vec{E} | \quad . \tag{A1.1}$$

For a plane wave incidence

$$J_z = 0 \tag{A1.2}$$

and following the cartesian notation used in Figure 5 (Chapter 2)

$$J_x = \sigma_1 E_{x'} \cos\theta + \sigma_2 E_{y'} \sin\theta$$

$$J_y = -\sigma_1 E_{x'} \sin\theta + \sigma_2 E_{y'} \cos\theta. \tag{A1.3}$$

The $E_{x'}$ and $E_{y'}$ can be written in terms of E_x and E_y

$$E_{x'} = E_x \cos\theta - E_y \sin\theta$$

$$E_{y'} = E_x \sin\theta + E_y \cos\theta \tag{A1.4}$$

From Equations (A1.3) and (A1.4), we write

$$J_x = \sigma_1 E_x \cos^2\theta - \sigma_1 E_y \cos\theta \sin\theta - E_x \sin^2\theta + \sigma_2 E_y \sin\theta \cos\theta$$

$$J_y = -\sigma_1 E_x \cos\theta \sin\theta + \sigma_1 E_y \sin^2\theta + \sigma_2 E_x \sin\theta \cos\theta + \sigma_2 E_y \cos^2\theta$$

(A1.5)

or, in matrix form

$$| \vec{J} | = | \sigma_{12} | \; | \vec{E} | \qquad \text{(A1.6)}$$

where

$$\sigma_{12} = \begin{vmatrix} \sigma_1 \cos^2\theta + \sigma_2 \sin^2\theta & (\sigma_2-\sigma_1) \sin\theta \cos\theta \\ (\sigma_2-\sigma_1) \sin\theta \cos\theta & \sigma_1 \sin^2\theta + \sigma_2 \cos^2\theta \end{vmatrix} . \qquad \text{(A1.7)}$$

Neglecting the displacement currents and taking the magnetic permeability of the medium as unity, from Maxwell's equations (in em system of units)

$$\begin{aligned} k\, E_y &= -\omega\, H_x \\ k\, E_x &= \omega\, H_y \\ -i\, k\, H_y &= 4\pi\, (\sigma_{11} E_x + \sigma_{12} E_y) \\ i\, k\, H_x &= 4\pi\, (\sigma_{12} E_x + \sigma_{22} E_y) \end{aligned} \qquad \text{(A1.8)}$$

where $i = \sqrt{-1}$, ω is the radian frequency and k is the propagation constant.

Solving for k from the set of equations (A1.8), we have

$$k^2 = \frac{4\pi i\omega}{2}\left[(\sigma_{11}+\sigma_{22}) \pm \left|(\sigma_{11}+\sigma_{22})^2 + 4(\sigma_{12}\sigma_{21} - \sigma_{11}\sigma_{22})\right|^{\frac{1}{2}}\right] \quad \text{(A1.9)}$$

Substituting $\sigma_{1,2}$ s from (A1.7), we get

$$k_1 = \pm (4\pi\sigma_1\omega)^{\frac{1}{2}} e^{i(\pi/4)}$$

$$k_2 = \pm (4\pi\sigma_2\omega)^{\frac{1}{2}} e^{i(\pi/4)} \quad \text{(A1.10)}$$

Thus there are two independent modes of propagation corresponding to two principal directions of anisotropy. Then the two skin depths are given by

$$p_1 = (2\pi\sigma_1\omega)^{-\frac{1}{2}}$$

$$p_2 = (2\pi\sigma_2\omega)^{-\frac{1}{2}} \quad \text{(A1.11)}$$

APPENDIX 2

A2.1. Fast Fourier Transform Algorithm

The Fast Fourier transform (FFT) algorithm is a method of computing the finite Fourier transform of a series of N (complex) data points in approximately N $\log_2$ N operations. The history (Cooley et al. 1967) of this algorithm can be traced back to the paper of Danielson and Lanczos in 1942. But it was not until Cooley and Tukey's (1965) paper it has attracted any attention. Following Cooley and Tukey's paper, Gentleman and Sande (1966), Bingham et al. (1967) and Welch (1967) have pointed out the usefulness of this algorithm for a variety of problems, such as the calculation of auto and crosscovariances, auto and crosspower spectra etc. The basic algebra of the Fast Fourier transform is described here.

The Discrete Fourier transform (DFT) of a time series x(t) is defined as

$$X(W) = \sum_{t=0}^{N-1} x(t) \; e^{(-2 \pi i \frac{t W}{N})} \qquad \text{(A2.1)}$$

where N is the number of points.

For algebraic convenience we write

$$e^{2 \pi i Y} = e(Y). \qquad \text{(A2.2)}$$

e(Y) = 1 if Y is an integer.

Equation (A2.1) can be written as

$$X(W) = \sum_{t=0}^{N-1} x(t) \quad e\left(\frac{tW}{N}\right) \qquad (A2.3)$$

Supposing N has factors G and H so that N = GH, and writing W = a' + b'G and t = b + aH, Equation (A2.3) can be transformed to

$$X(a'+b'G) = \sum_{b=0}^{H-1} \sum_{a=0}^{G-1} x\ (b+aH)\ e\left(\frac{-\ a'+b'G\quad b+aH}{GH}\right)$$

$$= \sum_{b=0}^{H-1} \sum_{a=0}^{G-1} x\ (b+aH)\ e\left(\frac{-a'b}{GH} - \frac{a'a}{G} - \frac{b'b}{H} - ab'\right)$$

$$= \sum_{b=0}^{H-1} \sum_{a=0}^{G-1} x\ (b+aH)\ e\left(\frac{-a'b}{GH}\right)\ e\left(\frac{-aa'}{G}\right)\ e\left(\frac{-bb'}{H}\right)$$

and since ab' is an integer so that e(ab') = 1

$$= \sum_{b=0}^{H-1} e\left(\frac{-bb'}{H}\right)\ e\left(\frac{-a'b}{GH}\right) \sum_{a=0}^{G-1} x\ (b+aH)\ e\left(\frac{-aa'}{G}\right) \qquad (A2.4)$$

To obtain the Fourier transform of the complete series, the inner sum of length G need be evaluated for only H different values of b, and G different values of a' requiring G.HG multiplications; then the outer sum, which is of length H

need be computed for H values of b', and G values of a' using H.GH multiplications. Thus the evaluation of the Fourier transform at all GH = N points requires (G + H)N multiplications. The conventional methods require N^2 multiplications. If $N = G_1\ G_2\ G_3\ G_4\ \ldots\ G$, then $(G_1 + G_2 + G_3 + G_4 + \ldots + G)N$ multiples suffice. In particular, if $N = 2^n$, one can compute the complete set of Fourier coefficients using $2nN = 2N \log_2 N$ multiplications. For example, if $N = 1024 = 2^{10}$, then $2N \log_2 N = 20480$, while $N^2 = 1048576$ which is 50 times 20480.

A2.2 Convolution and Covariance

The convolution of two time series in discrete form is defined as the inverse Fourier transform of the product of the Fourier transforms

$$\sum_{\tau=0}^{N-1} x(\tau)\ y(t-\tau) = \frac{1}{N} \sum_{W=0}^{N-1} X(W)\ Y(W)\ e^{\frac{2\ \pi\ i\ t\ W}{N}}$$

The convolution here must be cyclic.

Sande (1965) has shown that the autocovariance

$$R_{xx}(\tau) = \frac{1}{N} \sum_{t=0}^{N-\tau-1} x(t)\ x(t+\tau) \qquad \tau = 0, 1 \ldots \text{Lags}$$

and the crosscovariance

$$R_{xy}(\tau) = \frac{1}{N} \sum_{t=0}^{N-\tau-1} x(t)\ y(t+\tau) \qquad \tau = 0, 1 \ldots \text{Lags}$$

can be computed more economically by applying numerical convolution techniques rather than summing the lagged products. But the coveriances are not circular and the length of the series N may not be convenient for using Fast Fourier transform. Both these difficulties can be eliminated by extending each of the series by an appropriate number of zeros. Thus extending x series by N'-N zeros, one gets a new series such that

$$x'(t) = x(t) \qquad t = 0, 1 \ldots N$$

$$x'(t) = 0 \qquad t = N+1 \ldots N'$$

and similarly for y series. Then the Fourier transforms of both series, using the notation (A2.2) can be written as

$$X'(W) = \sum_{t=0}^{N'-1} x'(t) \quad e\left(\frac{-tW}{N'}\right)$$

$$Y'(W) = \sum_{s=0}^{N'-1} y'(s) \quad e\left(\frac{-sW}{N'}\right)$$

The inverse transform of the series formed by the product of the Y' and the complex conjugate of X' is written as

$$C(\tau) = \frac{1}{N'} \left\{ \sum_{W=0}^{N'-1} (X'^*(W) \quad Y(W))^* \; e\left(\frac{-W\tau}{N'}\right) \right\}^*$$

$$= \frac{1}{N'} \sum_{W=0}^{N'-1} X'^*(W) \; Y(W) \; e\left(\frac{W\tau}{N'}\right)$$

$$= \frac{1}{N'} \sum_{W=0}^{N'-1} \sum_{t=0}^{N'-1} \sum_{s=0}^{N'-1} x'^*(t)\ y'(s)\ e\left(\frac{W\tau}{N'}\right)\ e\left(\frac{tW}{N}\right)\ e\left(\frac{-sW}{N}\right)$$

$$= \frac{1}{N'} \sum_{t=0}^{N'-1} \sum_{s=0}^{N'-1} x'^*(t)\ y'(s) \sum_{W=0}^{N'-1} e\left(\frac{-W(s-t-\tau)}{N'}\right)$$

$$= \sum_{t=0}^{N'-1} \sum_{s=0}^{N'-1} x'^*(t)\ y'(s)\ {}_{N'}\ (s-t-\tau)$$

where $N'\ \delta_{N'}(s-t-\tau) = \sum_{t=0}^{N'-1} e^{\frac{-2\ \pi\ i\ (W-W')}{N'}}$

where $\delta_{N'}\ (KN) = 1$, for integer K, otherwise $\delta_{N'} = 0$,

therefore $C(\tau) = \sum_{t=0}^{N'-1} x'^*(t)\ y'(t + \tau)$.

In the time series problem the series are real, therefore

$$C(\tau) = \sum_{t=0}^{N'-1} x'(t)\ y'(t + \tau). \qquad \text{(A2.5)}$$

For $\tau < N' - N$, this is just N times the crosscovariance R_{xy}. The same steps can also be applied to the autocovariance. Thus the crosscovariance (or autocovariances) can be obtained by taking the inverse Fourier transform of the products of Fourier transforms of the series and finally dividing by the number of points in the series.

APPENDIX 3

A3.1. Apparent Resistivity Curves for Layered Anisotropic Earth Models

In this section the apparent resistivity curves for a few 3- and 4-layered anisotropic earth models are given for various values of θ, the angle from the major axis of anistropy to the axis of measurement x (Figure 7).

The following notation is used on the plots

curve	θ
a	40°
b	20°
c	0°
d	-20°

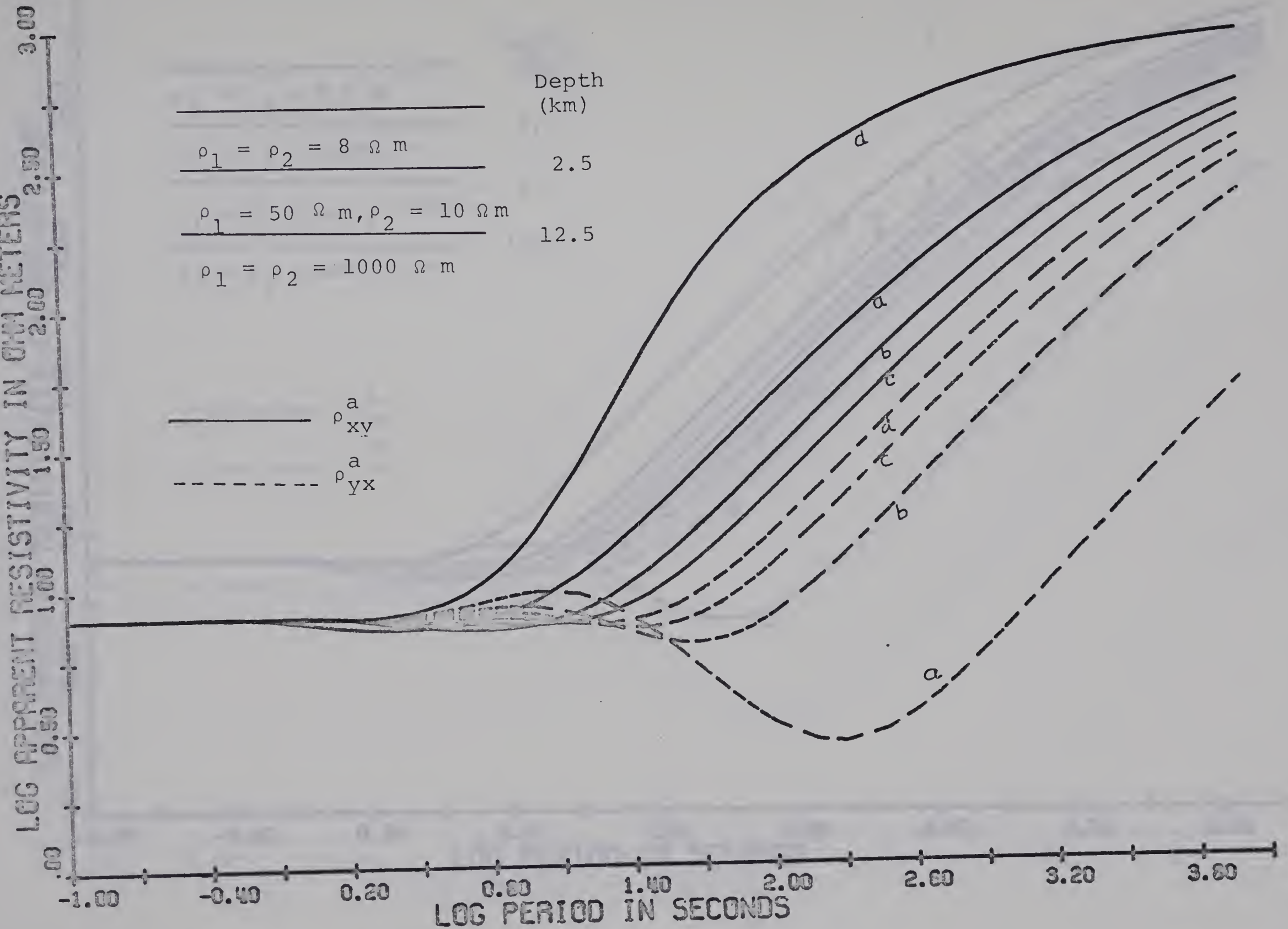
Depth (km)
$\rho_1 = \rho_2 = 8\ \Omega$ m
2.5
$\rho_1 = 50\ \Omega$ m, $\rho_2 = 10\ \Omega$ m
12.5
$\rho_1 = \rho_2 = 1000\ \Omega$ m
ρ^a_{xy}
ρ^a_{yx}
d
a
b
c
d
c
b
a
LOG APPARENT RESISTIVITY IN OHM METERS
.00
0.50
1.00
1.50
2.00
2.50
3.00
-1.00
-0.40
0.20
0.80
1.40
2.00
2.60
3.20
3.60
LOG PERIOD IN SECONDS

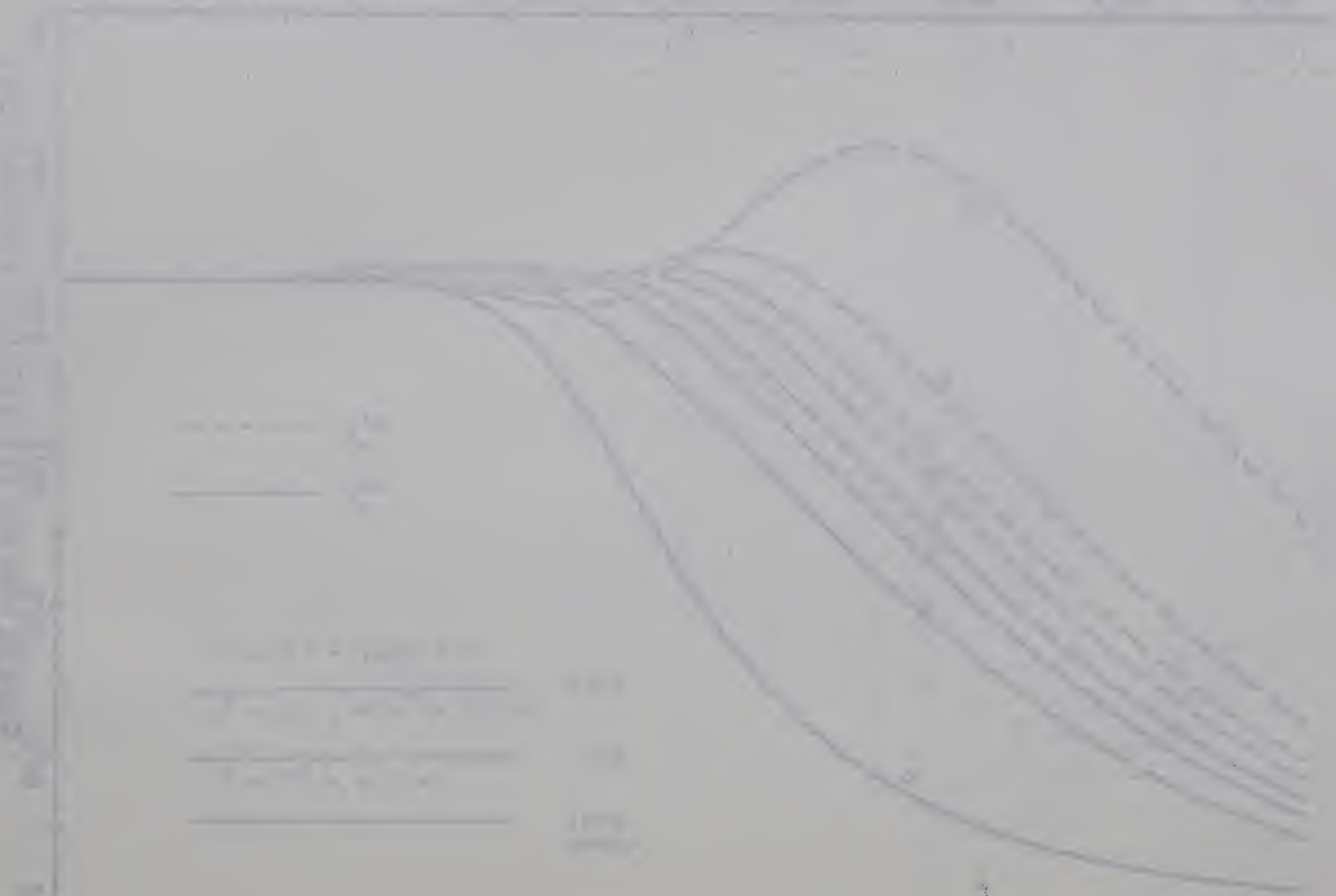

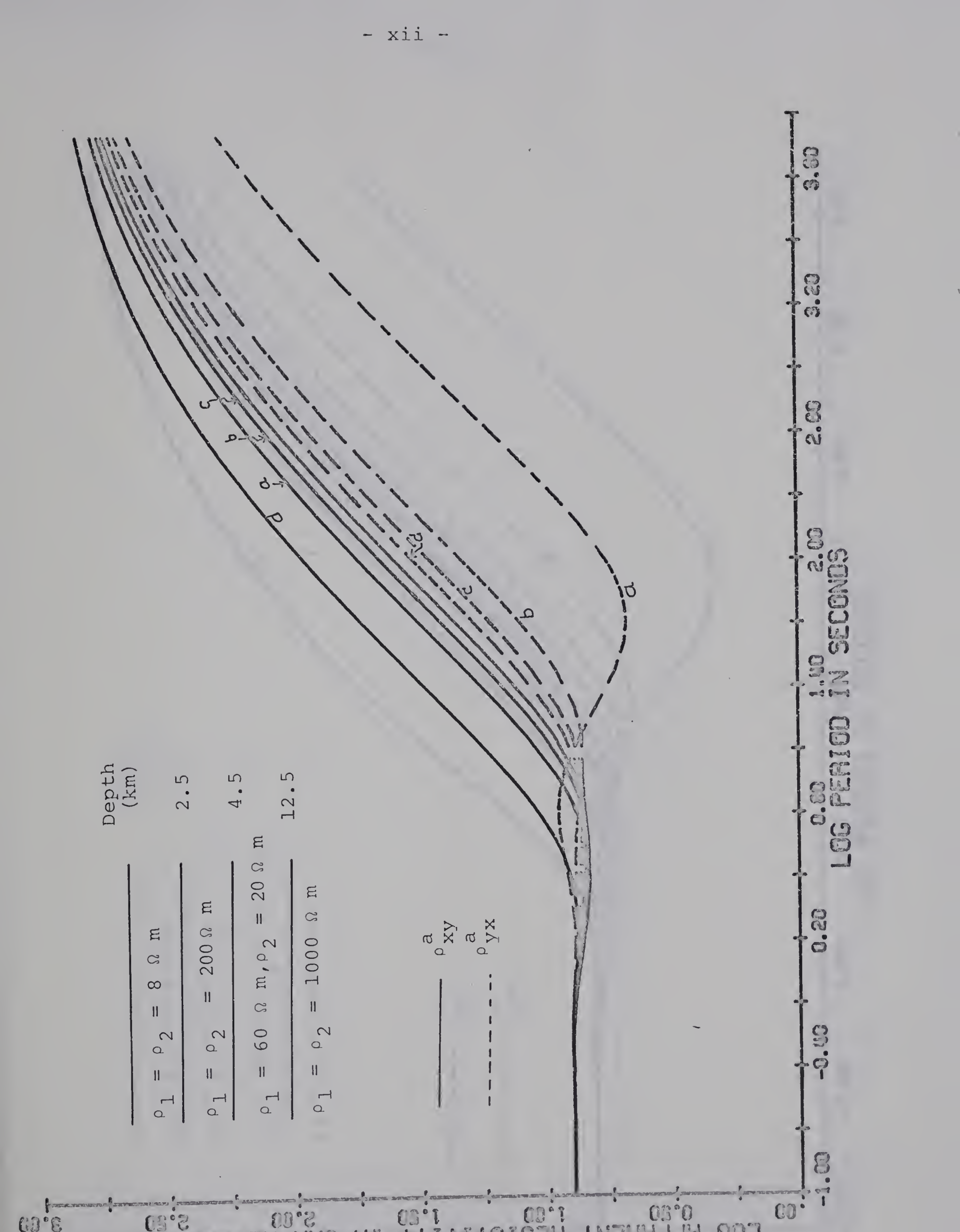
LOG APPARENT RESISTIVITY IN OHM METERS
3.00
2.50
2.00
1.50
1.00
0.50
.00
-1.00
-0.40
0.20
0.80
1.40
2.00
2.60
3.20
3.80
LOG PERIOD IN SECONDS
ρ^a_{xy}
ρ^a_{yx}
Depth (km)
$\rho_1 = \rho_2 = 8\ \Omega$ m
2.5
$\rho_1 = \rho_2 = 200\ \Omega$ m
4.5
$\rho_1 = 60\ \Omega$ m, $\rho_2 = 20\ \Omega$ m
12.5
$\rho_1 = \rho_2 = 1000\ \Omega$ m
p
q
r
s
t
u

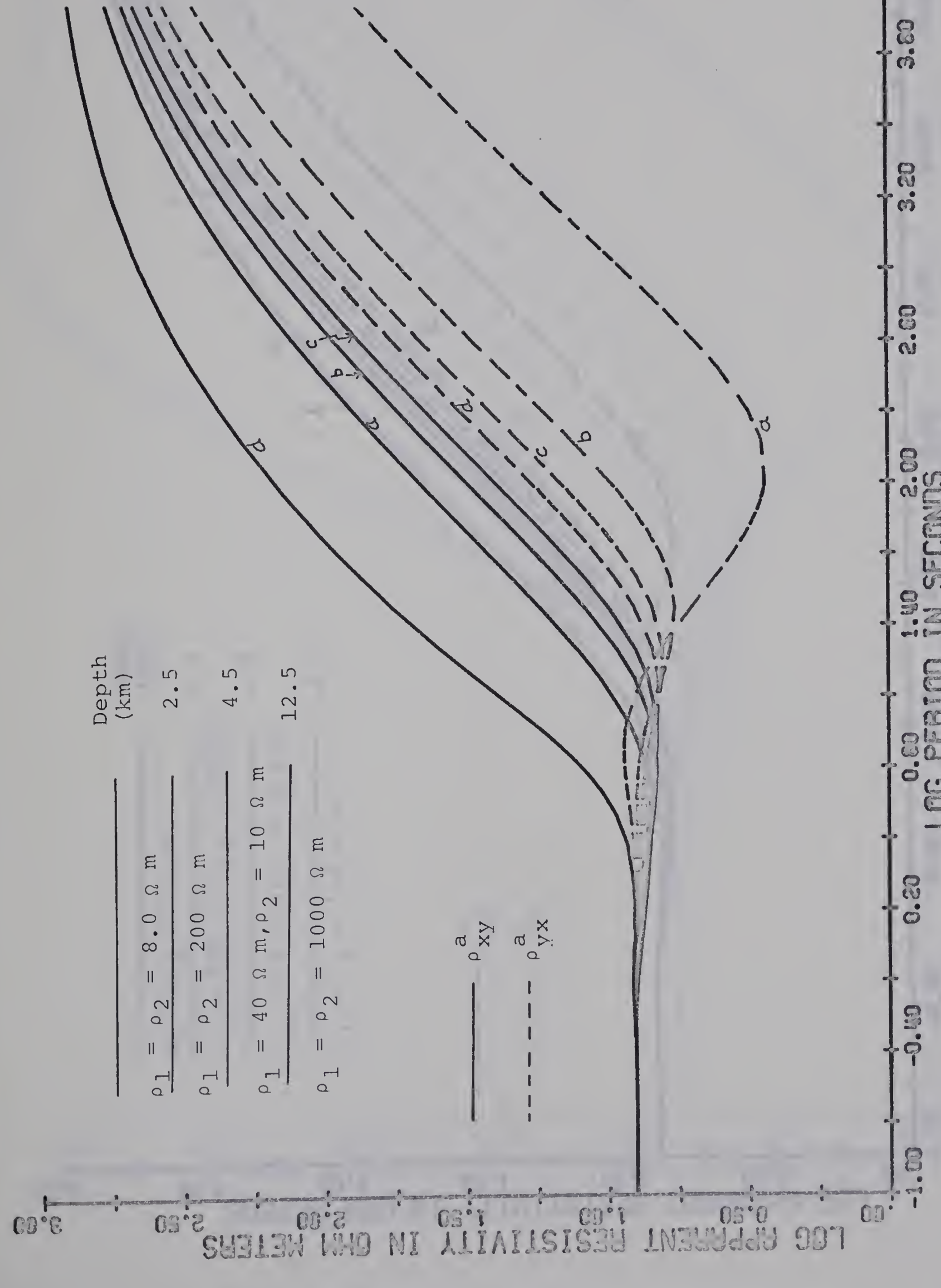
LOG APPARENT RESISTIVITY IN OHM METERS
3.00
2.50
2.00
1.50
1.00
0.50
00
-1.00
-0.50
0.00
0.20
0.40
0.60
LOG PERIOD IN SECONDS
2.00
3.20
3.00
ρ_a
ρ_1
ρ_2
ρ_3
ρ_4
ρ_5
ρ_6
ρ_a xy
ρ_a yx
Depth (km)
$\rho_1 = \rho_2$ = 8.0 Ω m
2.5
$\rho_1 = \rho_2$ = 200 Ω m
4.5
ρ_1 = 40 Ω m, ρ_2 = 10 Ω m
12.5
$\rho_1 = \rho_2$ = 1000 Ω m

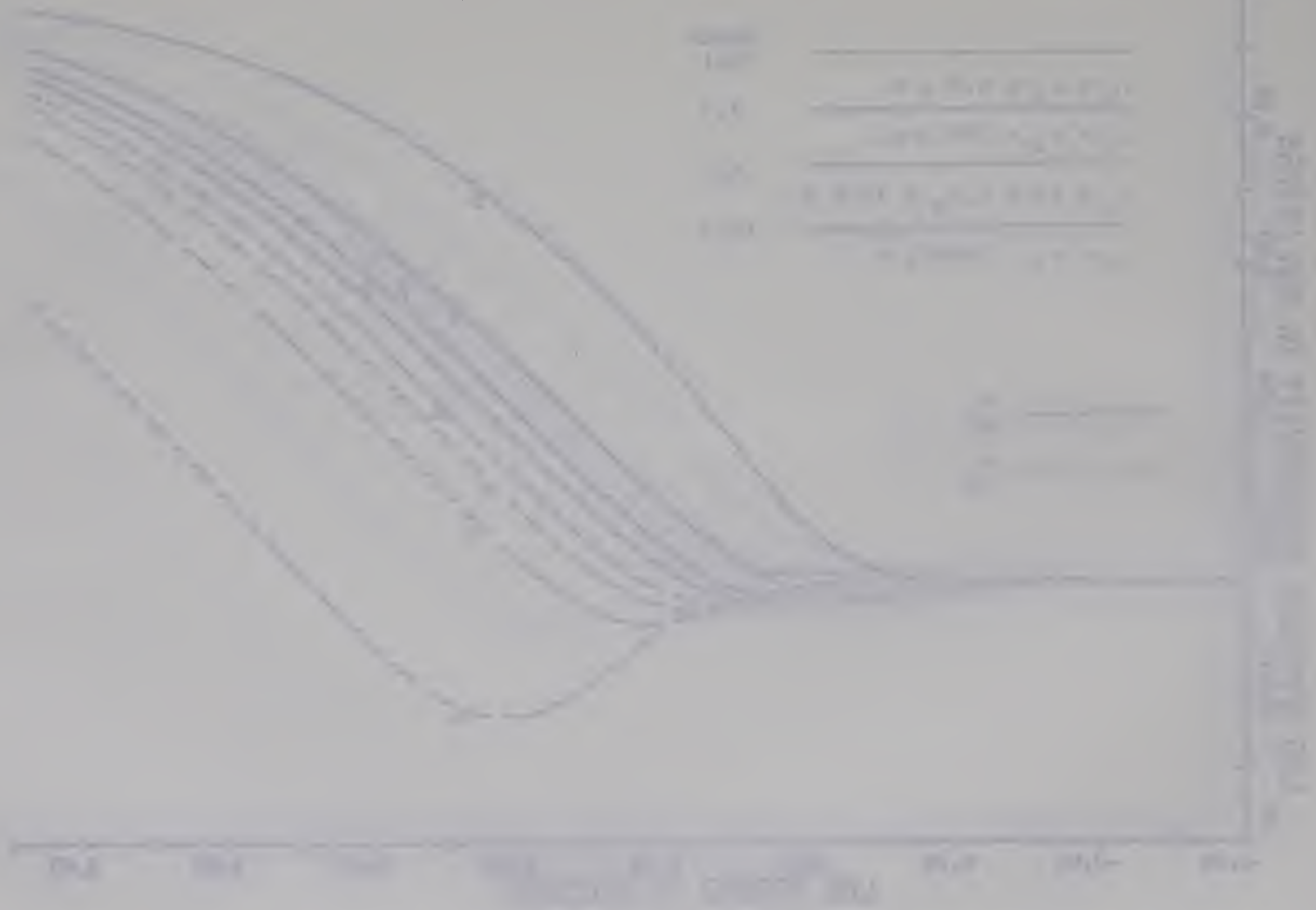

	Depth (km)
$\rho_1 = \rho_2 = 8\ \Omega$ m	2.5
$\rho_1 = 400\ \Omega$ m, $\rho_2 = 200\ \Omega$ m	4.5
$\rho_1 = 60\ \Omega$ m, $\rho_2 = 30\ \Omega$ m	14.5
$\rho_1 = \rho_2 = 100\ \Omega$ m	

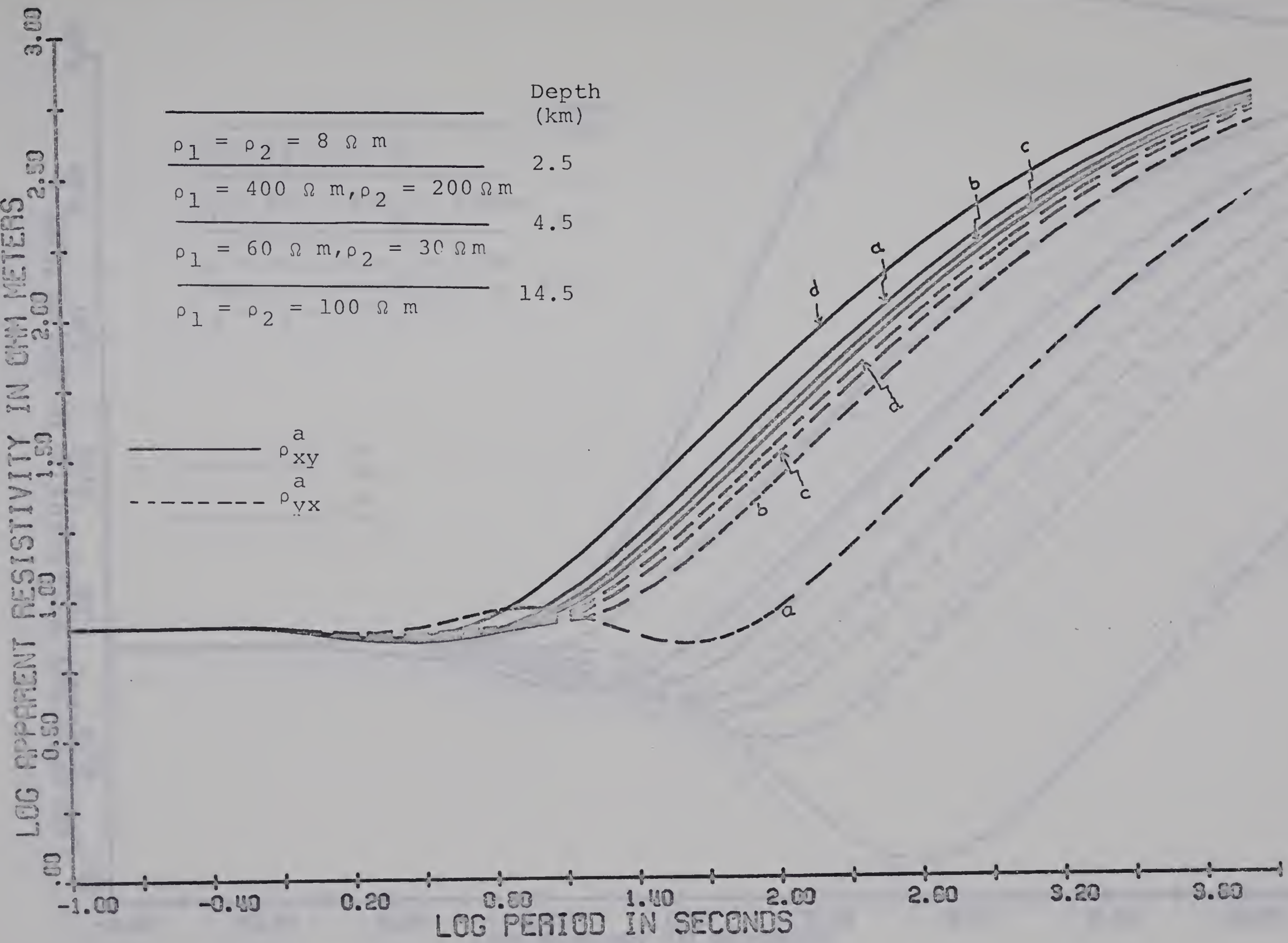

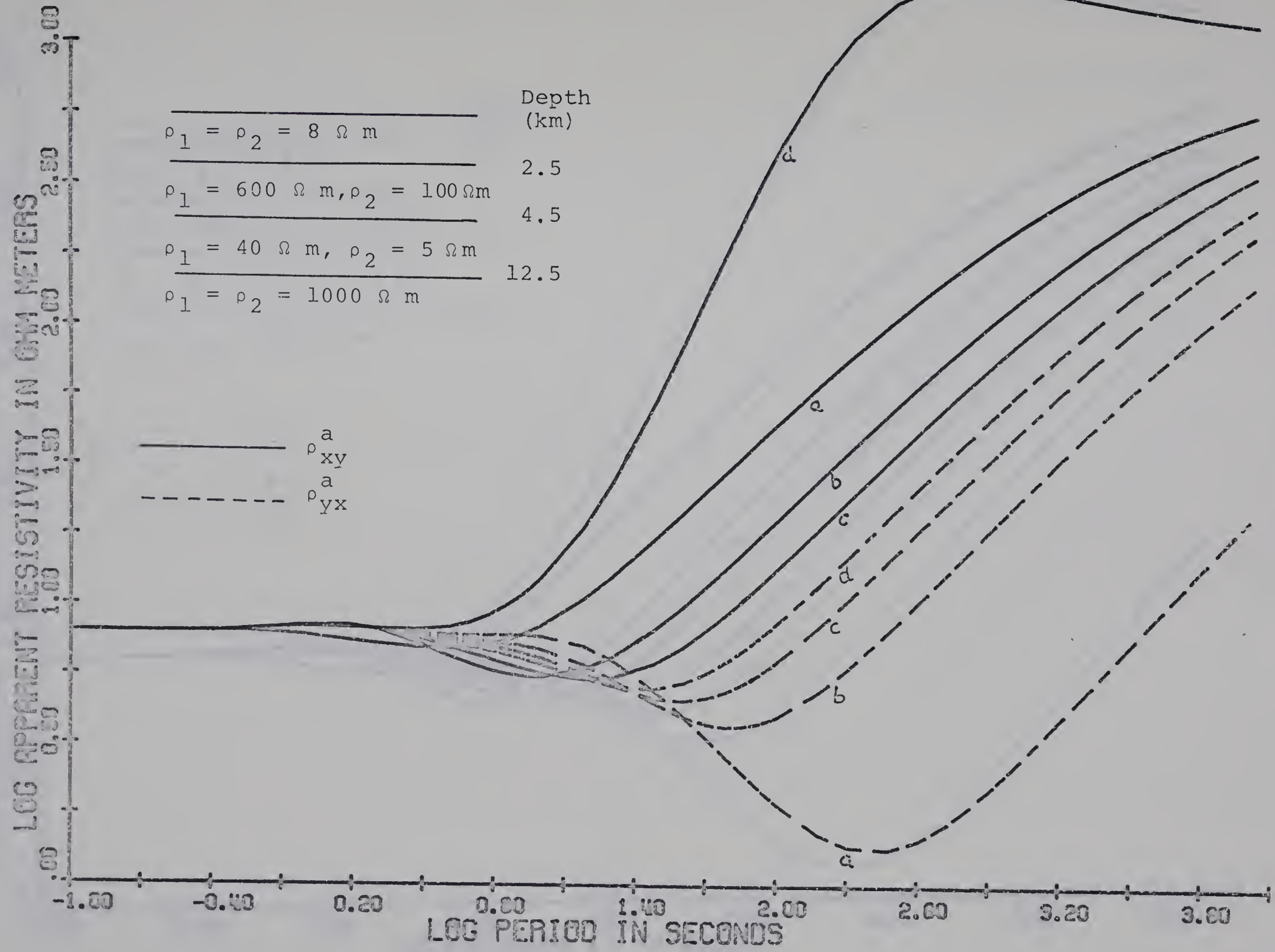
Depth (km)
$\rho_1 = \rho_2 = 8\ \Omega$ m
2.5
$\rho_1 = 600\ \Omega$ m, $\rho_2 = 100\ \Omega$m
4.5
$\rho_1 = 40\ \Omega$ m, $\rho_2 = 5\ \Omega$m
12.5
$\rho_1 = \rho_2 = 1000\ \Omega$ m
ρ^a_{xy}
ρ^a_{yx}
a
b
c
d
LOG APPARENT RESISTIVITY IN OHM METERS
.00
0.50
1.00
1.50
2.00
2.50
3.00
-1.00
-0.40
0.20
0.80
1.40
2.00
2.60
3.20
3.80
LOG PERIOD IN SECONDS

	Depth (km)
$\rho_1 = \rho_2 = 8\ \Omega$ m	2.5
$\rho_1 = 400\ \Omega$ m, $\rho_2 = 100\ \Omega$m	4.5
$\rho_1 = 80\ \Omega$ m, $\rho_2 = 5\ \Omega$m	12.5
$\rho_1 = \rho_2 = 1000\ \Omega$ m	

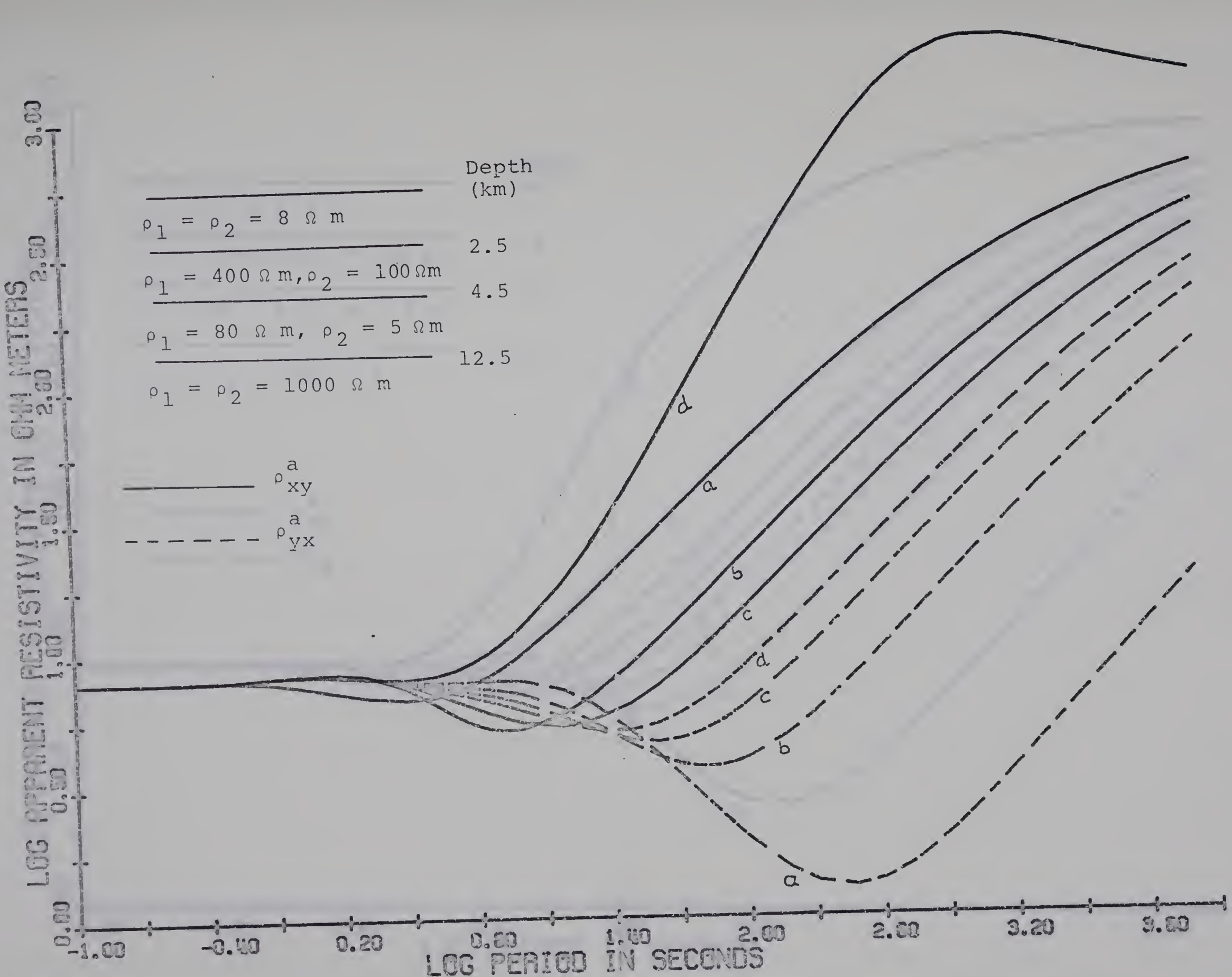

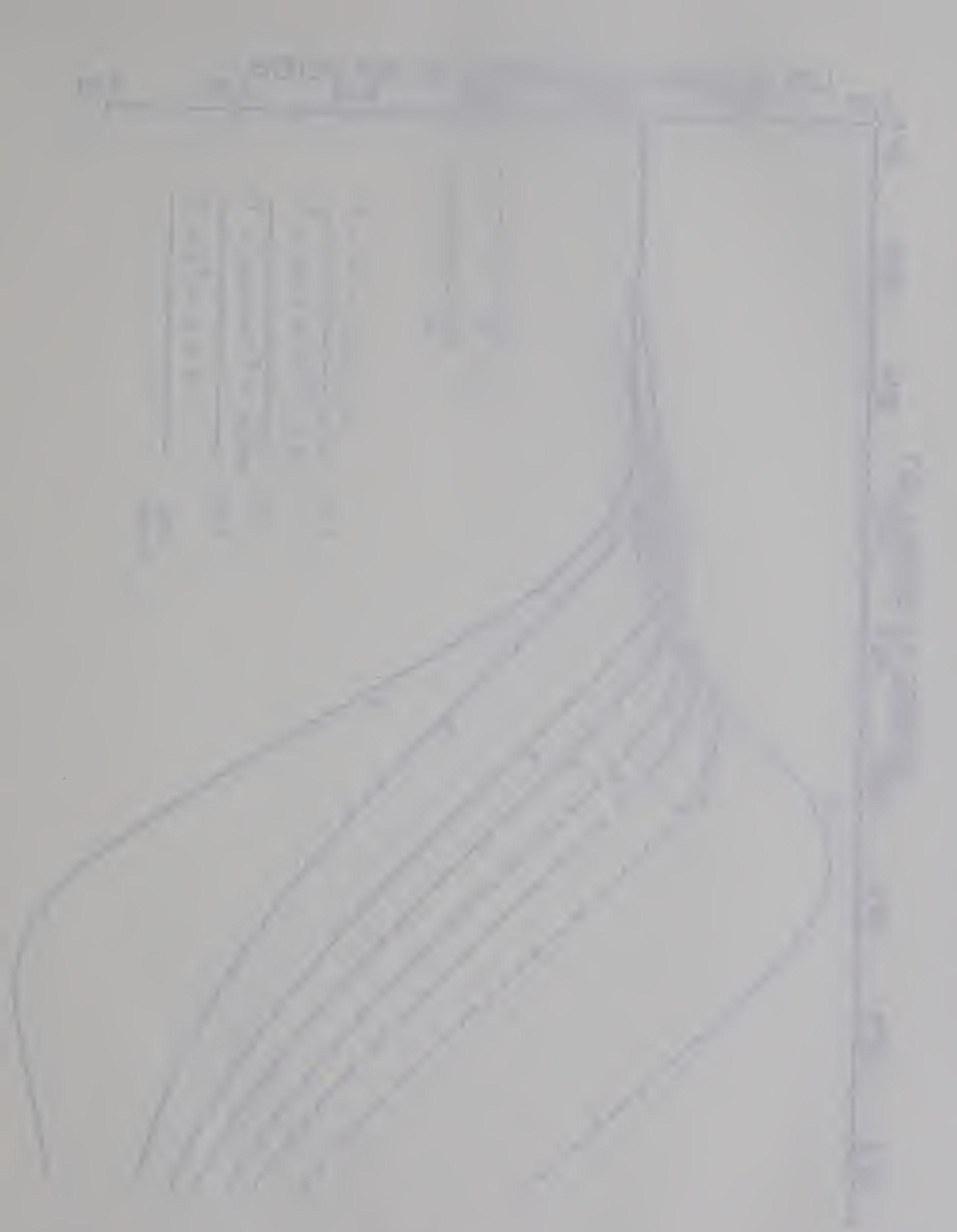

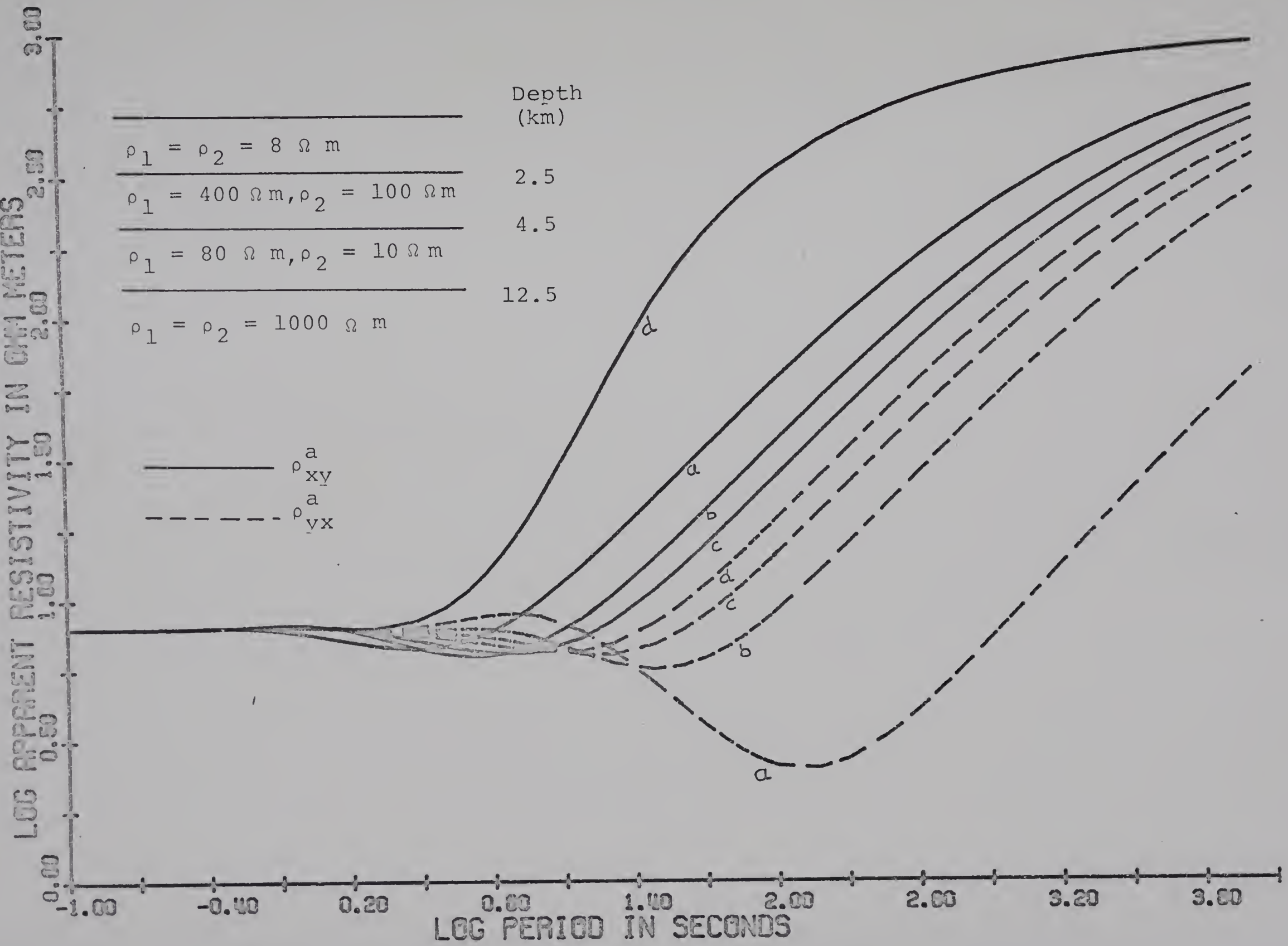
Depth (km)
$\rho_1 = \rho_2 = 8\ \Omega$ m
2.5
$\rho_1 = 400\ \Omega$m, $\rho_2 = 100\ \Omega$m
4.5
$\rho_1 = 80\ \Omega$ m, $\rho_2 = 10\ \Omega$m
12.5
$\rho_1 = \rho_2 = 1000\ \Omega$ m
ρ^a_{xy}
ρ^a_{yx}
LOG APPARENT RESISTIVITY IN OHM METERS
0.00
0.50
1.00
2.00
3.00
-1.00
-0.40
0.20
0.80
1.40
2.00
2.60
3.20
3.80
LOG PERIOD IN SECONDS